

# Design of a 6U CubeSat for an Ionospheric Science Mission

A Major Qualifying Project Report  
Submitted to the Faculty of the  
WORCESTER POLYTECHNIC INSTITUTE  
in Partial Fulfillment of the Requirements for the  
Degree of Bachelor of Science  
in Aerospace Engineering

by



---

Tyler Lizotte



---

Harrison Smith

March 15, 2022

Approved by



---

Nikolaos A. Gatsonis, Advisor

Professor, Aerospace Engineering Department

## **Abstract**

This project presents the thermal and environmental analysis of a 6U CubeSat designed for ionospheric composition measurements on a 180-600 km elliptical orbit. Thermal analysis with the Systems Tool Kit (STK) and COMSOL software shows that components temperatures are within requirements. Surface charging analysis using the Space Plasma Interaction System (SPIS) software shows low surface potentials under nominal ambient plasma conditions. The total radiation dosage, micrometeorite and space debris impact fluxes evaluated with STK's Space Environment and Effects Tool (SEET) present minimal risks. The magnetic fields induced by the magnetic torquers may require repositioning of the magnetometers. This project also presents the design and fabrication of a Helmholtz cage for future testing.

## **Acknowledgements**

The authors would like to thank Professor Nikolaos A. Gatsonis for advising this project and Professor Zachary Taillefer, and Professor Michael A. Demetriou who advised the two other projects and formed the Appleton Project. The authors would also like to thank the previous MQP members Alexander Klenk and Sydney Messey for their assistance on the Helmholtz cage.

## Table of Authorship

1.0 Introduction	ALL
1.1 Overview of WPI Projects on CubeSats	ALL
1.2 Appleton Project Goals	ALL
1.3 Appleton Design Requirements, Constraints, and Considerations	ALL
1.3.1 Subsystem Requirements	ALL
1.3.2 Design Constraints	ALL
1.4 Appleton Project Management and the Systems Engineering Group	ALL
1.5 MQP Objectives, Approach and Standards	ALL
1.6 Gantt Chart	ALL
2.0 Science Payload	TL
2.1 Mini-Ion Neutral Mass Spectrometer (INMS)	TL
2.2 Gridded Retarding Ion Drift Sensor (GRIDS)	TL
3.0 Thermal Analysis and Design	HS
3.1 Thermal Background	HS
3.2 Thermal Analysis Methods	HS
3.3 Results, Discussion, and Design Considerations	HS
4.0 Analysis and Design Considerations for Space Plasma, Radiation and Debris Environment Interactions	TL
4.1 Ionosphere Overview	TL
4.2 Surface Charging Analysis and Design Considerations	TL
4.3 Analysis of Induced Magnetic Fields Effects and Design Consideration	TL
4.4 Analysis of Radiation Effects and Design Considerations	TL
4.5 Analysis of Micrometeorite and Space Debris Effects and Design Considerations	TL
5.0 Helmholtz Cage	ALL
5.1 Past Project Work	TL
5.2 Updating the DAQ	ALL
5.3 Updating the Power Supplies	ALL
5.4 The I2C Interface	ALL
6.0 Conclusions, Recommendations, and Social Impact	ALL
6.1 Conclusions	ALL
6.2 Recommendations	ALL
6.2.1 Thermal Recommendations	HS
6.2.2 Space Environment Recommendations	TL
6.3 Social Impact – Space Debris	ALL
Appendix A: STK to COMSOL MATLAB Code	HS
Appendix B: Helmholtz Cage Instruction Manual	ALL

# Table of Contents

Abstract.....	2
Acknowledgements.....	3
Table of Authorship .....	4
Table of Contents .....	5
List of Figures .....	7
List of Tables .....	9
1. Introduction .....	10
1.1 Overview of WPI Projects on CubeSats .....	11
1.2 Appleton Project Goals .....	13
1.3 Appleton Design Requirements, Constraints, and Considerations .....	13
Subsystem Requirements.....	13
Design Constraints.....	15
1.4 Appleton Project Management and the Systems Engineering Group .....	18
1.5 MQP Objectives, Approach and Standards.....	19
Thermal Analysis and Design.....	19
Space Environment Analysis and Design.....	19
1.6 Gantt Chart .....	20
2. Science Payload.....	21
2.1 Mini-Ion Neutral Mass Spectrometer (INMS).....	21
2.2 Gridded Retarding Ion Drift Sensor (GRIDS) .....	25
3. Thermal Analysis and Design.....	29
3.1 Thermal Background .....	29
3.2 Thermal Analysis Methods.....	30
3.3 Results, Discussion, and Design Considerations .....	37
4. Analysis and Design Considerations for Space Plasma, Radiation and Debris Environment Interactions.....	40
4.1 Ionosphere Overview .....	40
4.2 Surface Charging Analysis and Design Considerations .....	43
4.3 Analysis of Induced Magnetic Fields Effects and Design Considerations .....	51
4.4 Analysis of Radiation Effects and Design Considerations .....	54
4.5 Analysis of Micrometeorite and Space Debris Effects and Design Considerations .....	59

5. Helmholtz Cage .....	62
5.1 Review of Previous Work.....	62
5.2 Updating the DAQ .....	66
5.3 Updating Power Supplies.....	67
5.4 The I2C interface .....	68
6. Conclusions, Recommendations, and Social Impacts .....	69
6.1 Conclusions .....	69
6.2 Recommendations for Future Work.....	70
6.3 Thermal Recommendations.....	70
6.4 Space Environment Recommendations.....	70
6.5 Social Impact – Space Debris.....	71
7. References .....	73
8. Appendix A: STK to COMSOL MATLAB Code.....	76
9. Appendix B: Helmholtz Cage Instruction Manual .....	77

## List of Figures

Figure 1: Appleton CubeSat with solar panels deployed	10
Figure 2: Gated Time-of-Flight (TOF) Apparatus (Rodriguez et al., 2016)	23
Figure 3: Counts of detected masses according to their TOF (Rodriguez et al., 2016)	23
Figure 4: The Mini-INMS species collection system (Rodriguez et al., 2016)	24
Figure 5: Initial Ion Measurements from the INMS aboard NASA Dellingr (Hatfield, 2018)	25
Figure 6: The GRIDS apparatus (Hatfield, 2018)	27
Figure 7: Grids within the GRIDS system (Hatfield, 2018)	27
Figure 8: Appleton with Solar Vector Tracking from STK SEET simulation	33
Figure 9: SolidWorks model of Appleton with exposed internals	34
Figure 10: Defeatured COMSOL model of Appleton	35
Figure 11: Set Up of COMSOL Heat Flux	36
Figure 12: Set Up of COMSOL Heat Source	37
Figure 13: Appleton Average surface temperature ( $^{\circ}\text{C}$ ) over 24 hours from STK SEET simulation	37
Figure 14: Appleton surface temperatures (K) from COMSOL with the Anti-Nadir (-Y) and Wake (-Z) showing	38
Figure 15: Appleton thermal analysis with Nadir (Y) and RAM (Z) sides showing	39
Figure 16: Appleton temperature from COMSOL with Sun Facing Side (X) showing	39
Figure 17: Appleton Thermal Analysis (Internals Exposed)	39
Figure 18: Interaction between the Ionosphere and Different Radio Wave Frequencies (Space Weather Prediction Center)	41
Figure 19: Layers of the Ionosphere and their altitudes relative to sea level (UCAR Center for Science and Education)	42
Figure 20: Plasma interactions with spacecraft surfaces (Garrett and Whittlesey, 2012)	44
Figure 21: Thickness of Aluminum shielding capable of absorbing certain energy levels (Garrett and Whittlesey, 2012)	45
Figure 22: Solar Activity, measured by sunspots, across recent Solar Cycles	46
Figure 23: Surface materials of Appleton's 6U bus (excluding solar panels)	48
Figure 24: Simplified GMESH model of Appleton's 6U bus, excluding and including a single solar array panel	48
Figure 25: 6U CubeSat surface potentials (V) for fully conductive and grounded surface from SPIS	49
Figure 26: 6U CubeSat surface potentials (V) for fully conductive and grounded surface with a single solar array	50
Figure 27: The location of Appleton's primary systems. In the ADCS block, the magnetorquer is located at the geometric center of the CubeSat	52
Figure 28: Magnetic flux density (Tesla) within the 6U CubeSat induced by the operation of a magnetorquer from COMSOL simulation	53
Figure 29: Accumulated Radiation Dosage or Total Ionizing Dosage (TID) over Appleton's scientific mission duration from STK: SEET radiation simulation	55
Figure 30: Integral Flux of hydrogen protons vs. energy levels over the Appleton mission duration from STK: SEET GCR simulation	56
Figure 31: SEP Probability vs Fluence level over the Appleton mission duration from STK: SEET SEP simulation	58
Figure 32: SEP Probability vs Fluence for various mission durations (AGI, 2020)	59

Figure 33: Impact Flux and Damaging Flux over the mission duration for an Aluminum Target	60
Figure 34: Impact Flux and Damaging Flux over the Appleton mission duration for a Mylar target from STK: SEET particle simulations	61
Figure 35: Helmholtz cage design (Brown et al. 2021)	63
Figure 36: Helmholtz magnetic field strength along the centerline for a single coil pair (Brown et al., 2021)	64
Figure 37: Helmholtz cage magnetic field test (Brown et al., 2021)	66
Figure 38: Chip in International Space Station Cupola window (ESA, 2016).	72
Figure 39: NO and JOE	79
Figure 40: PAUL or SMOL connected to NO and JOE	79
Figure 41: SMOL and PAUL connected to NO and JOE	80
Figure 42: FRED or TED added to frame	80
Figure 43: Full frame assembly	81
Figure 44: Bracket and rubber pieces	81
Figure 45: Splitter	82
Figure 46: LabView – LabJack panel window	83

## List of Tables

Table 1: Project Gantt Chart	20
Table 2: Parameters and performance of the Mini-INMS (Klenzing et al., 2019; Rodriguez et al., 2016)	22
Table 3: Parameters and performance of the GRIDS (Rodriguez et al., 2016; Davidson et al., 2019)	26
Table 4: Thermal Limits of Appleton's Components	31
Table 5: Maximum Heat Generation by Each Component	32
Table 6: Positional Parameters of Appleton above the North Pole	46
Table 7: IRI Outputs for Sept.2010	47
Table 8: Maximum Impact and Mass Flux for Space Particulates over the mission duration	61

## 1. Introduction

This Major Qualifying Project (MQP) presents the analysis of the thermal and space environment aspects for the design of Appleton, a 6U CubeSat for an ionospheric science mission, and the continuing development of a Helmholtz cage for ground based magnetic experiments on CubeSat components. Appleton, shown in Figure 1, utilizes the NASA-designed miniature Ion Neutral Mass Spectrometer (mini-INMS) and Gridded Retarding Ion Drift Sensor (GRIDS) to measure the composition of the ionosphere's F layer.



Figure 1: Appleton CubeSat with solar panels deployed.

The mission goal is to further the understanding of the ionosphere by analyzing its composition, local properties, and providing data to investigate any present anomalies. The CubeSat was given the name of ‘Appleton’, after Sir Edward Victor Appleton, the physicist who won the Nobel Prize in physics for the discovery of the Ionosphere (The Nobel Prize, 2022). Appleton operates in a semi-Sun-synchronous elliptical orbit with a perigee of 180 km and apogee of 600 km where it will collect data relevant to its mission objective.

This MQP group worked on the Appleton Project alongside partner MQP groups in the form of a Systems Engineering Group (SEG). The groups are referenced below according to the section they contributed to. The goals of the overall Appleton Project are two:

First, to design and ensure the functionality of Appleton for its mission duration of one year. The design was accomplished by the three MQP groups by addressing all the primary systems of the Appleton CubeSat that include mechanical (Durgin et al., 2022), attitude determination and control (ADCS) (Gagnon et al., 2022), telemetry and communication (Gagnon et al., 2022), command and data handling (Gagnon et al., 2022), power (Durgin et al., 2022), propulsion (Durgin et al., 2022), payload integration, thermal, and environmental analysis. Payload integration, thermal analysis, and environmental analysis are addressed in this report.

Second, to continue the design and development of a Helmholtz Cage for the testing of the ADCS subsystem. The cage will be designed to replicate the magnetic environment of a low Earth orbit, such that a test of Appleton’s magnetorquer systems can be conducted.

## **1.1 Overview of WPI Projects on CubeSats**

CubeSats are small satellites that are designed for a variety of uses. CubeSats are comprised of 10 cm x 10 cm x 10 cm cubes, referred to as units or ‘U’ (Dumbar and Loff, 2018). CubeSats are

designated by the number of units they have, followed by the 'U', a 2U CubeSat would be 10 x 10 x 20 cm in size. Through the CubeSat Launch Initiative (CSLI), NASA promotes CubeSat development by education institutions and nonprofits, while also developing many of its own (Dumbar and Hill, 2020). Due to the small nature of CubeSats, they are more finically attainable than larger satellites. Their small design also allows them to be launched in a variety of ways. CubeSats are typically added on to launches for larger spacecraft or have dedicated ride-share launches. However, CubeSats have also been deployed by hand, as they were thrown into orbit by astronauts on the International Space Station (ISS) (NASA CSLI, 2017).

For several years, MQP teams at WPI have conducted CubeSat design projects. Teams have worked to design and analyze CubeSats for a variety of different mission requirements. The previous year's CubeSat MQP, ZAT 2102 (Brown et al., 2021) designed a 6U CubeSat, named MagSTARS, for the study of the F layer of the Ionosphere. Similar to this project, the CubeSat occupied a semi-Sun-synchronous orbit, however had a perigee of 250 km, and an apogee of 400 km. MagSTARS contained a single payload, the NASA designed Mini-Ion Neutral Mass Spectrometer (INMS). ZAT 2102 also started the development of the Helmholtz cage, by the creation of the magnetic coils and a data acquisition system.

This project conducts a different mission and is of a new design. However past projects were referenced by the team to build a base for Appleton's design. In 2020, MQP project NAD 2001 (Anderson et al., 2020) designed a 6U CubeSat for the study of extreme Low Earth Orbit (eLEO). The satellite contained the single payload mini-IMNS, similar to the next two years' projects. The team used software such as STK, COMSOL, ANSYS, and SolidWorks to analyze the CubeSats design.

## 1.2 Appleton Project Goals

- Perform the conceptual design and corresponding analyses for Appleton, a 6U CubeSat which carries the NASA-designed miniature Ion Neutral Mass Spectrometer (mini-INMS) and Gridded Retarding Ion Drift Sensor (GRIDS) to measure the composition of the ionosphere's F layer. The CubeSat is to be placed in a semi-Sun-synchronous elliptical orbit with a perigee of 180 km and apogee of 600 km where it will collect data relevant to its primary objective for a mission duration of one year.
- Continue previous MQP work on building and testing the Helmholtz cage. A Helmholtz cage is used for ground testing of the ADCS to verify its performance capabilities. It can generate a dynamic magnetic field that is meant to replicate the Earth's magnetic field such that interactions with the onboard magnetorquer can be tested.

## 1.3 Appleton Design Requirements, Constraints, and Considerations

### Subsystem Requirements

#### Payload Requirements:

- 1.1: The spacecraft shall be capable of assessing the local composition and state of the ionosphere.

#### Mechanical Requirements:

- 2.1: The spacecraft design must be compatible with the launch vehicle.
- 2.2: The spacecraft must be designed for the launch environment following the General Environmental Verification Standard (GEVS).

#### Propulsion Requirements:

- 3.1: The propulsion system shall be able to transfer the spacecraft from its initial parking orbit to the desired scientific orbit.
- 3.2: The propulsion system shall be able to counteract orbital perturbations in order to extend the mission lifetime.

#### Power Requirements:

- 4.1: Telemetry, propulsion, payload, thermal and attitude control, will be powered for mission duration.
- 4.2: System will be powered via solar panels and a battery.
- 4.3: Power will be reserved for end-of-life de-orbit.

#### Attitude Determination and Control Requirements:

- 5.1: The spacecraft shall achieve sufficient torque authority to overcome predicted disturbance torques from atmospheric drag, magnetic field influence, and thrust vector misalignment.

#### Telemetry and Communication Requirements:

- 6.1: The spacecraft shall have adequate data rate for command uplink over the orbital period.
- 6.2: The spacecraft shall have adequate data rate to downlink science data collected and stored.

#### Command and Data Handling Requirements:

- 7.1: The spacecraft shall have the computational capability for closed loop ADC.

#### Thermal Requirements:

- 8.1: The spacecraft shall be designed to operate in an ambient and self-induced thermal environment.

- 8.2: The thermal design shall provide temperatures within the following ranges: -  
20 – 50 °C.

#### Space Environment Requirements:

- 9.1: The spacecraft shall be designed to operate for mission lifetime within the ambient and self-induced electromagnetic environment.
- 9.2: The spacecraft shall be designed to operate for the mission lifetime within the ambient radiation environment.
- 9.3: The spacecraft shall be designed to operate for the mission lifetime within the ambient micrometeorite and space debris environment.

#### Helmholtz Design Requirements:

- 10.1: The spacecraft's ADCS shall be validated through ground-based testing to within +/- 5° margin of error.
- 10.2: Generated magnetic fields will be measured and controlled; capable of reproducing expected field strengths for our orbit.
- 10.3: The test article must be attached to a torque-free rigging system, i.e., an air bearing platform.

### **Design Constraints**

#### Payload Constraints:

- Both the Mini-Ion Neutral Mass Spectrometer (Mini-INMS) and Gridded Retarding Ion Drift Sensor (GRIDS) require RAM facing aperture orientation (+Z-axis in Figure 1)
- Total data collection rate of the payload is ~14 kbit/s, adequate data storage and transmission is required
- Functionality of the Mini-INMS ceases beyond the temperature range -10 to 50 °C
- Functionality of the GRIDS ceases beyond the temperature range -20 to 80 °C
- The payload requires a total power of 2.3 W for both devices
- The Mini-INMS and GRIDS require 1.3 U and 0.75 U of spacecraft volume, respectively

#### Mechanical Constraints:

- The weight of the CubeSat will not exceed 9.1 kg
- The spacecraft design must be compatible with the Canisterized Satellite Dispenser (CSD)

#### Propulsion Constraints:

- The propulsion system must be able to operate under the constraints set by the power and mechanical subsystems.

#### Power Constraints:

- Max thermal functional range -20 to 80 deg C

#### Attitude Determination and Control Constraints:

- The system shall maintain 3-axes of attitude knowledge better than 1 degree from apogee to perigee.
- The spacecraft shall use this torque authority to maintain a steady orientation of +/- 5 degrees off its pre-modeled nadir pointing attitude vector.
- The spacecraft shall achieve sufficient torque authority to overcome predicted disturbance torques from atmospheric drag, magnetic field influence, and thrust vector misalignment.

#### Telemetry and Communications Constraints:

- Spacecraft access time will be modeled to determine any additional constraints that are needed in the design
- Command and Data Handling Constraints:
- The spacecraft shall have data capacity for science data.

#### Thermal Constraints:

- The thermal environment will be modeled to determine appropriate thermal protection to protect each individual component.

#### Space Environment Constraints:

- Environmental effects will be modeled to determine whether additional constraints will be added to the design.

#### Helmholtz Cage Constraints:

- The Helmholtz cage must generate a reliable magnetic field in a volume large enough for a 6U test article
- The air bearing platform must provide consistent pressure capable of lifting the test article allowing for torque-free rotation

#### **1.4 Appleton Project Management and the Systems Engineering Group**

This MQP was completed in conjunction with two other MQP teams which focused on other systems of Appleton. Each separate MQP contained a grouping of subsystems. The MQP completed by Durgin et al. (2022) conducted the orbital/propulsion, mechanical, and power subsystem design. The MQP completed by Gagnon et al. (2022) completed the ADCS design, telemetry and communications, and command and data handling. While this MQP completed the thermal and space environment design. Each week every team met to hold a Systems Engineering Group (SEG) meeting to communicate the past weeks' work with each other and to seek advice from advisors. Throughout the entire project, the project manager role rotated so that every member involved in the project gained experience in that role. With the collaboration and analyses of all three teams, the 6U Appleton was designed to complete an Ionospheric mission to gather data on particle densities in the atmosphere in order to study anomalies in the Ionosphere. In addition to the design and analysis of a CubeSat the three MQP teams also continued the work of previous year's MQP ZAT-2102 focusing on the development of a Helmholtz cage and air bearing platform for the testing of attitude determination and control systems (ADCS). All three project teams work simultaneously to complete the design and analysis of Appleton.

## 1.5 MQP Objectives, Approach and Standards

### Thermal Analysis and Design

- The objective of the thermal subsystem analysis and design is to address the Design Requirements 8.1 and 8.2 and propose mitigation strategies, if necessary.
- Approach and Standards
  - [8.1] Evaluate thermal loads onto Appleton from the Sun during a typical orbit as well as the reflecting light from the Earth, using STK's Space Environment and Effects Tool (SEET).
  - [8.2] Use thermal loads as inputs to COMSOL and perform thermal analysis using a de-featured CAD model of Appleton.
  - [8.1, 8.2] Use the predicted temperature profiles and ensure that design requirements are met.
  - [8.1, 8.2] Evaluate internal thermal loads created by Appleton's components using COMSOL.

### Space Environment Analysis and Design

- The objective of the space environment analysis and design is address the Design Requirements 9.1, 9.2, and 9.3.
- Approach and Standards
  - [9.1]: Evaluate the impact of the plasma environment on surface charging using the Space Plasma Interaction System (SPIS) software. Evaluate any surface potentials (Volts) that develop and their impact on Appleton's systems.

- [9.1]: Evaluate the induced magnetic fields from the magnetorquers using COMSOL. Use the predicted values to assess potential impact on magnetometers onboard Appleton.
- [9.2, 9.3]: Evaluate the total radiation dosage as well as micrometeorite and space debris impacts using the Space Environment and Effects Tool (SEET) program in STK. Use the results of the simulation to determine if any additional radiation or particulate shielding is necessary.

### 1.6 Gantt Chart

Table 1 below shows the Gantt Chart the team used to plan out design and analysis of Appleton.

Table 1: Project Gantt Chart

	Week 1	Week 2	Week 3	Week 4	Week 5	Week 6	Week 7	Week 8	Week 9	Week 10	Week 11	Week 12	Week 13	Week 14	Week 15	Week 16	Week 17	Week 18	Week 19	Week 20	Week 21	Week 22	Week 23	Week 24	
Thermal Research	█	█	█	█	█																				
STK Thermal Analysis & Data Collection					█	█	█	█	█	█															
COMSOL Thermal Analysis									█	█	█	█	█	█	█	█	█	█	█	█					
Final Thermal Protection Design and Testing																									
Space Environment Research	█	█	█	█																					
Spacecraft Charging Analysis			█	█	█	█	█	█	█	█	█	█	█	█	█	█	█	█	█	█					
STK Radiation Analysis																									
STK Particle Impacts Analysis																									
COMSOL Magnetorquer Model																									
Final Report Write-Up																									

## **2. Science Payload**

The goal of Appleton's mission is to analyze the ionosphere across the F1 and F2 layers by collecting data regarding the local composition and state of the ionic and neutral species. To accomplish this, two separate devices, the Mini-Ion Neutral Mass Spectrometer (Mini-INMS) and Gridded Retarding Ion Drift Sensor (GRIDS) were selected. Both instruments, when used in tandem, provide measurements of the densities of neutral and ionized species in the ionosphere, as well as relative ion concentrations, temperatures, and velocity vectors (component normal to instrument face). In this section we present these instruments focusing on characteristics that impact the Appleton design.

### **2.1 Mini-Ion Neutral Mass Spectrometer (INMS)**

NASA Goddard's Mini-INMS can provide in situ density measurements of ion and neutral species in the ionosphere. Specifically, it can measure densities of the species shown in Table 2.

Table 2: Parameters and performance of the Mini-INMS (Klenzing et al., 2019; Rodriguez et al., 2016).

<b>Parameter</b>	<b>Performance</b>
Ion Species	H <sup>+</sup> , He <sup>+</sup> , N <sup>+</sup> , O <sup>+</sup> , NO <sup>+</sup> , O <sub>2</sub> <sup>+</sup>
Ion Range	10 <sup>3</sup> cm <sup>-3</sup> to 10 <sup>7</sup> cm <sup>-3</sup>
Neutral Species	H, He, N, O, N <sub>2</sub> , O <sub>2</sub>
Neutral Range	10 <sup>5</sup> cm <sup>-3</sup> to 10 <sup>9</sup> cm <sup>-3</sup>
Volume	1.3 U
Mass	960 g
Power	1.8 W
Cadence	1 s
Data Rate	13.1 kbit/s
Operating Temperature	-10 to 50 °C
FOV	±20° x ±10° around ram

The Mini-INMS measures these densities using a gated time-of-flight (TOF) instrument as shown in Figure 2. Both the neutral and ion apertures use this instrument to measure the mass of each species according to their TOF.

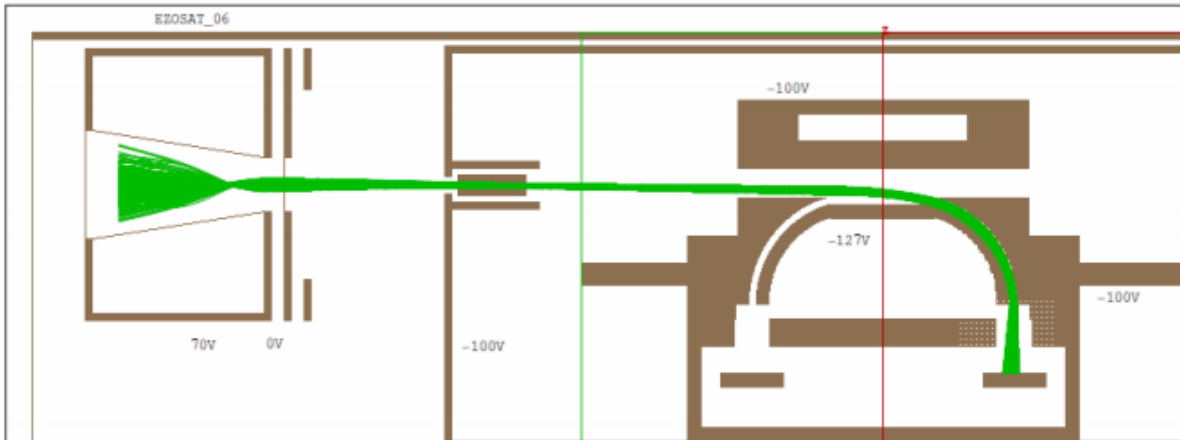


Figure 2: Gated Time-of-Flight (TOF) Apparatus (Rodriguez et al., 2016).

On the ion side, particles enter the aperture and receive a pre-acceleration voltage which brings all ions to a similar energy level. While the energy of incoming ions will vary, the voltage applied is orders of magnitude greater, thereby negating this difference. With all ions having the same kinetic energy their velocity into the instrument will be solely dependent on the particle mass; heavier ions will travel more slowly than lighter ions. The faster moving ions will have a smaller time of flight (TOF) than heavier ions; by ordering ions in their velocity according to their mass a TOF model can be created for the collection period, as shown in Figure 3.

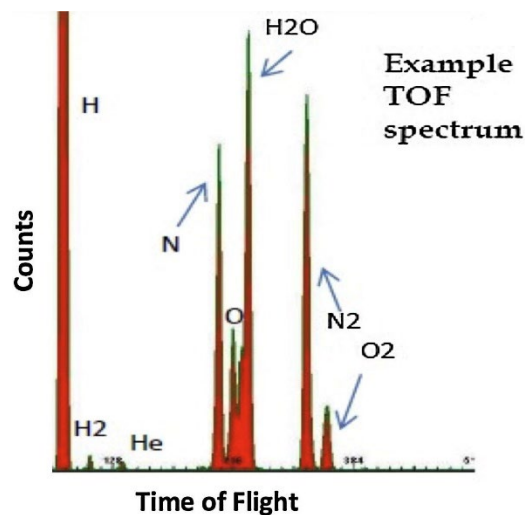


Figure 3: Counts of detected masses according to their TOF (Rodriguez et al., 2016)

Similarly, on the neutral side, particles are also given an initial pre-acceleration voltage to use the same TOF methods as on the ion side. The main difference between the two is that the neutral side also contains an ion repellant at the aperture to only allow neutral particles entry. In this way the densities of both the ionized and neutral species can be measured. The entire apparatus is shown in Figure 4.

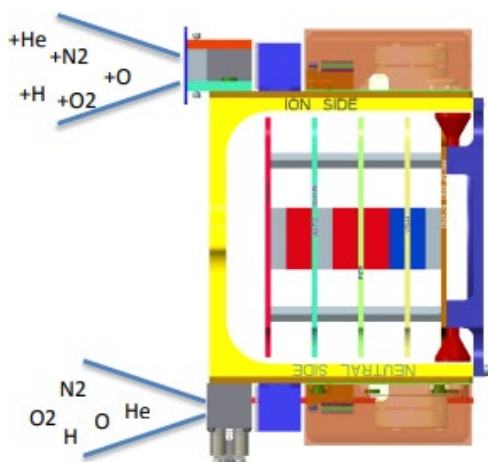


Figure 4: The Mini-INMS species collection system (Rodriguez et al., 2016).

The functionality of the INMS has been proven in multiple missions including ExoCube, Dellingr, and petitSat. The ExoCube, flown in 2015, was the first flight of the Mini-INMS. However, due to inadequate antenna deployment on the CubeSat the data received was less than desired. The instrument functioned well and was able to send TOF spectrums that aligned with those predicted, such as the sample shown in Figure 3, but ultimately communication with the CubeSat was lost (Rodriguez et al., 2016). Unfortunate circumstances also occurred with the NASA Dellingr spacecraft, launched in 2017. The CubeSat was accidentally powered before deployment resulting in a dead battery from the start of the mission (Hatfield, 2018). However, the

CubeSat was able to recover using its solar panels. After the outgassing of any particles remaining in the INMS from Earth's atmosphere, the satellite was able to successfully activate and record data from the ion side of the INMS as shown in Figure 5. Data from the neutral side of the INMS has not been able to be demonstrated by this mission.

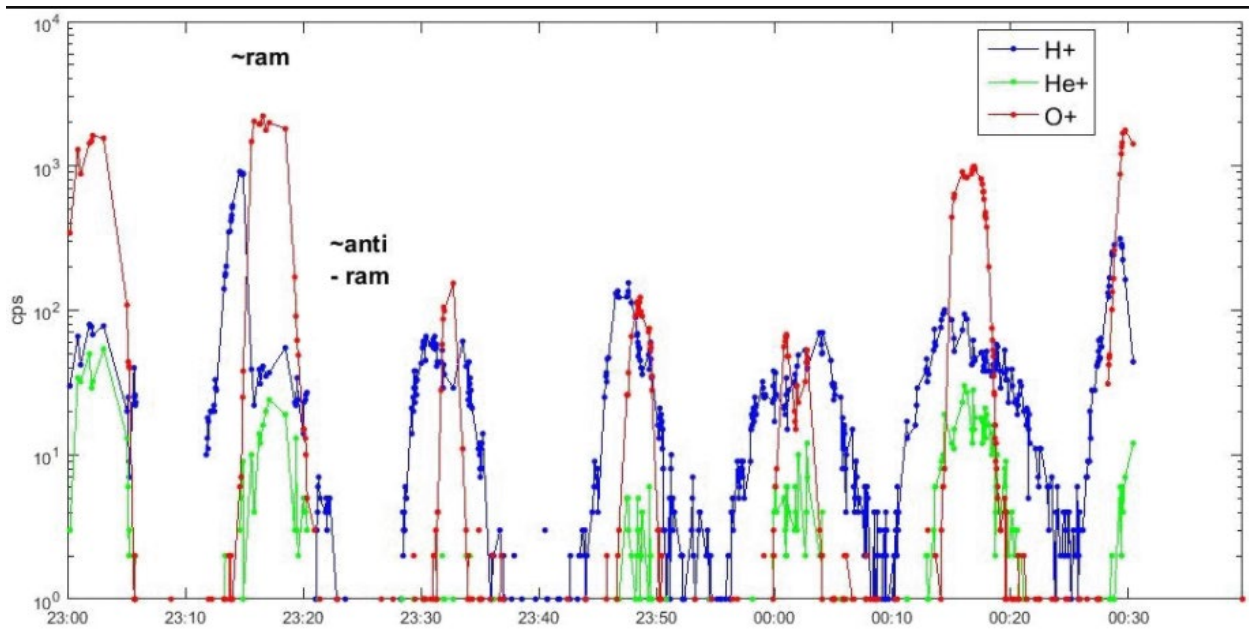


Figure 5: Initial Ion Measurements from the INMS aboard NASA Dellingr (Hatfield, 2018).

## 2.2 Gridded Retarding Ion Drift Sensor (GRIDS)

The GRIDS system can provide in-situ ion density, temperature, relative concentration of heavy to light ions, and the component of the velocity vector normal to the instrument face. Specifically, it can measure the parameters shown in Table 3. (Rodriguez et al., 2016; Davidson et al., 2019)

Table 3: Parameters and performance of the GRIDS (Rodriguez et al., 2016; Davidson et al., 2019).

Parameter	Performance
Velocity Range (Accuracy)	-1500 m/s to 1500 m/s ( $\pm 10$ m/s)
Ion Species	H <sup>+</sup> , He <sup>+</sup> , O <sup>+</sup>
Ion Density Range (Accuracy)	$5 \times 10^3 \text{ cm}^{-3}$ to $5 \times 10^7 \text{ cm}^{-3}$ ( $500 \text{ cm}^{-3}$ or 2%)
Ion Temperature Range (Accuracy)	0 K to 3000 K (10 K or 5%)
Ion Composition Range (Accuracy)	0 to 1 (0.02)
Volume	0.75 U
Mass	500 g
Power	0.5 W
Cadence	0.5 Hz
Data Rate	533 bit/s
Operating Temperature	-20 to 80 °C

The GRIDS device is made of a series of biased and grounded grids located behind a RAM facing aperture. These grids are supplied with a retarding voltage to act as ion-energy filters (Hatfield, 2018). At the back of the instrument there are ion collectors which detect currents produced from ion impacts. By varying the retarding voltage in the aperture grids the ion species can be selectively allowed to pass through and into the collectors. Current from ions impacting the collector is used to calculate total ion flux as a function of retarding voltage (Hatfield, 2018). From this calculation the ion density, temperature, relative concentration of heavy to light ions, and the

component of the velocity vector normal to the instrument face can be derived. The grids sensor and the breakdown of its internal grids are shown in Figures 6 and 7.

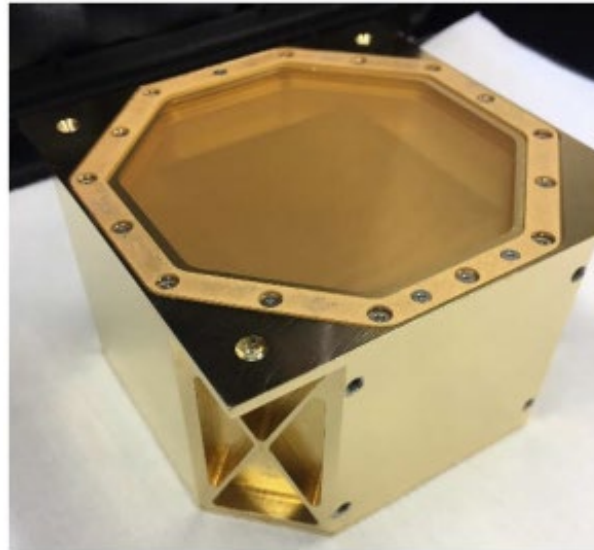


Figure 6: The GRIDS apparatus (Davidson et al., 2020).

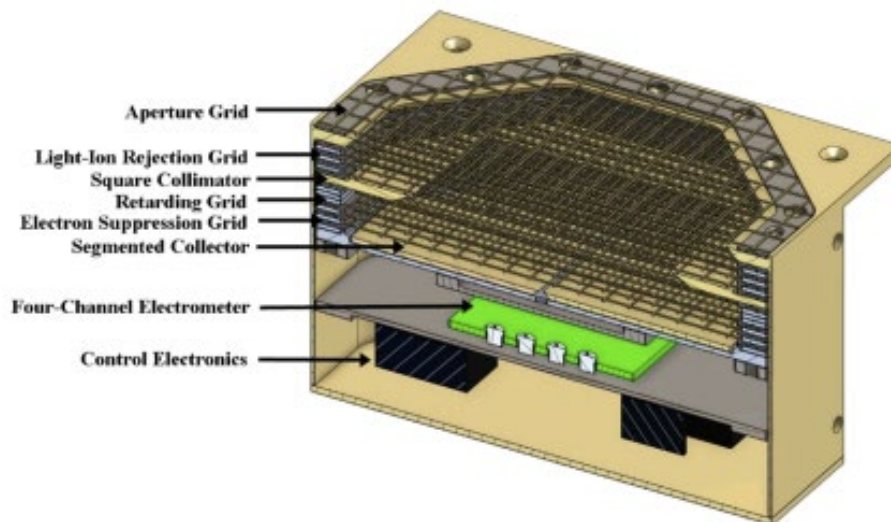


Figure 7: Grids within the GRIDS system (Davidson et al., 2020).

The GRIDS system and the Mini-INMS were both selected for the petitSat mission, deploying from the ISS in 2021, this mission will help determine the link between plasma enhancements and medium-sized traveling ionospheric disturbances (MSTIDs) (Keesey, 2017).

### 3. Thermal Analysis and Design

Appleton surfaces and internal components must maintain temperatures as set by the thermal design requirements. Thermal analysis and design are performed using a combination of Systems Tool Kit Space Environment Effects Tool (STK SEET) and COMSOL Multiphysics. This section outlines the methodology, analysis, and results of the thermal design process to meet the thermal design requirements.

#### 3.1 Thermal Background

In the ambient Low Earth Orbit (LEO) environment, there are three main factors that must be considered when performing the thermal analysis for a spacecraft: 1. solar flux, which is the power per unit area emitted by the sun over the entire electromagnetic spectrum and received by the spacecraft (in  $W/m^2$ ); 2. Earth's blackbody radiation, which is the thermal power per unit area emitted by the Earth and received by the spacecraft (in  $W/m^2$ ); and 3. Earth's albedo, which is the fraction of solar energy that that Earth reflects (measured from 0-1). Because of the daily, seasonal, and yearly variation of these variables, average values for the three factors considered in the thermal analysis. This is done to reduce the number of simulations during thermal design. In ZAT2102 (Brown et al, 2021) it was shown that little to no difference in the temperature ranges of the spacecraft surfaces when they calculated a "hot cycle", or "cold cycle" based off the maximum and minimum values of each environmental factor, and it was recommended that similar project use yearly average values to simplify the simulations. In Appleton's thermal analysis the following average yearly values were used for the ambient thermal inputs: the solar flux constant was taken as  $1367 W/m^2$  on a surface perpendicular to the solar rays, Earth's blackbody radiation value of  $231 W/m^2$ , and an albedo fraction of 0.30 (NASA Earth Observatory [EO]; Boushon, 2018; Hyun Ko et al, 2017; Bograd, 2018).

As spacecraft operates, Appleton induces its own thermal environment that must be accounted for. The internal components of Appleton dissipate heat a result of not being 100% efficient, and the effects of the dissipated heat must be analyzed to ensure they do not negatively affect Appleton's operation. Following along with previous MQPs, an electrical efficiency of 90% or 0.9 was assumed for all the active components (Anderson et al, 2020). The amount of heat generated by the components is needed to ensure that the spacecraft remains inside of its survivability temperatures.

To achieve the thermal design requirements of a spacecraft, engineers rely on both passive and active thermal control methods. A passive thermal control method is one that does not require power supplied by the spacecraft. Examples of passive control methods are radiators and surface finishes. A radiator dissipates heat through a panel on the exterior of the spacecraft with a high emissivity. Surface finishing allows for the spacecraft to become either more or less reflective to emit thermal energy (Brown et al, 2021). An example of an active method of thermal control is a heater. A heater uses the power supplied by the spacecraft to generate heat that is dissipated to the component that it is attached to and the surrounding environment. It is typical to see these heaters attached to batteries as they are more sensitive to colder temperatures (Hyun Ko et al, 2017; Brown et al, 2021). For Appleton, a passive thermal control method is preferred as it reduces the complexity of the design by not having to power and control another subsystem.

### **3.2 Thermal Analysis Methods**

The first step in thermal analysis of Appleton is to determine the upper and lower thermal limits that the spacecraft can endure. Manufacturer provided data sheets of each component in Appleton were consulted to gather two temperature ranges, the survivability range, and the optimum operating range. When either, or both, temperature ranges were not provided by the

manufacturer, the standard temperature range for commercial electronics of -40 – 85 °C was used (Coker, 2014) remaining in line with previous years reports. Table 4 below lays out the values for each of the components used. Based off the thermal ranges of the components chosen, the thermal limit range was set to be -20 – 50 °C.

Table 4: Thermal Limits of Appleton’s Components.

<b>Component</b>	<b>Operating Temp (°C)</b>	<b>Survivability Temp (°C)</b>
Antenna	-20 – 50	-40 – 85
Mini-INMS	-10 – 50	-40 – 85
GRIDS	-20 – 80	-40 – 85
Battery	-10 – 50	-40 – 85
ADCS Subsystem Sensors	-40 – 85	-40 – 85
Transceiver	-40 – 85	-40 – 85
Control Board/Computer	-40 – 80	-40 – 85

The next task in Appleton’s thermal analysis is to determine the amount of heat generated by the internal components of Appleton. As the components in Appleton use power, they are not 100% efficient, and some of their power is lost as heat to the environment. The heat dissipated by each component  $P_{dis}$  is given in terms of the power delivered to the component  $P_{del}$  by

$$P_{dis} = N \cdot P_{del} \tag{1}$$

Where  $N$  in Eq. (1) represents inefficiency of the component in terms of a percentage. Every component was assumed to have an efficiency of 90% setting  $N = 0.1$  following (Brown et al, 2021) as little information is provided by manufacturers regarding the efficiency of

components. The amount of power that was used to calculate the heat generation for each component was set to be its maximum power usage throughout the duration of the mission. This ensured that any heat generated by the components would be accounted for in the thermal simulations. The maximum amount of heat generated by each component can be seen in Table 5 below.

Table 5: Maximum Heat Generation by Each Component.

Component	$P_{del}$ , Power Delivered (W)	$P_{dis}$ , Power Dissipated (W)
Mini-INMS	1.8	0.18
GRIDS	0.5	0.05
Control Board/Computer	1	0.1
Transceiver	0.5	0.05
Antenna	0.01	0.01
Propulsion	65	6.5
ADCS Subsystem Sensors	4.5	4.5

After any internal heat generation was determined, the thermal solar effects on Appleton were determined using STK SEET. Using the orbit determined by the propulsion sub-team (Durgin et al, 2022), the solar vector was tracked over the period of the orbit along with the solar intensity. Solar intensity was measured on a scale from 0 to 100. In STK SEET, the side of the spacecraft that was sun facing throughout the duration of the mission was set as a “plate” with an area of 0.02 m<sup>2</sup>. The plate was then locked to the axis perpendicular to the ram-facing side of the satellite so it would be in sight of the sun throughout the orbit. Figure 8 below shows the satellite in its orbit as

the solar vector is tracked. The satellite shown is the standard image for satellites within STK, it does not visually represent Appleton, nor influence the analysis.



Figure 8: Appleton with Solar Vector Tracking from STK SEET simulation.

The solar vector data was then extracted from STK as a Microsoft Excel csv file, along with the solar intensity data. This file contained the  $x, y, z$  components for the solar vector, and time of Appleton in the orbit. The file was then imported into MATLAB. Inside of MATLAB the solar intensity data was normalized by dividing it by 100 and the time stamp was converted to total seconds in the orbit. Additionally, the solar vector data was separated into six separate files for the six different directions of the solar vector (positive  $x$ , positive  $y$ , positive  $z$ , negative  $x$ , negative  $y$ , and negative  $z$ ). The code used to do this was developed for previous MQPs and can be found in Appendix A (Anderson, 2020). By separating all the files, it prepares the files to be imported into COMSOL Multiphysics.

After importing the solar vector and intensity data into COMSOL, the 3D SolidWorks model of Appleton developed by the Mechanical subsystem was imported as well. When the data was imported into COMSOL, it was imported as an interpolation function, as the data exported by STK was in the form of discrete points. The SolidWorks model was imported as an assembly to keep the dimensions the same.

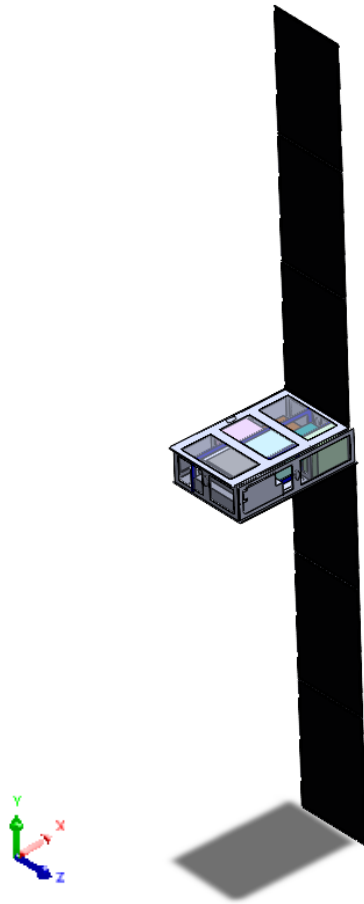


Figure 9: SolidWorks model of Appleton with exposed internals.

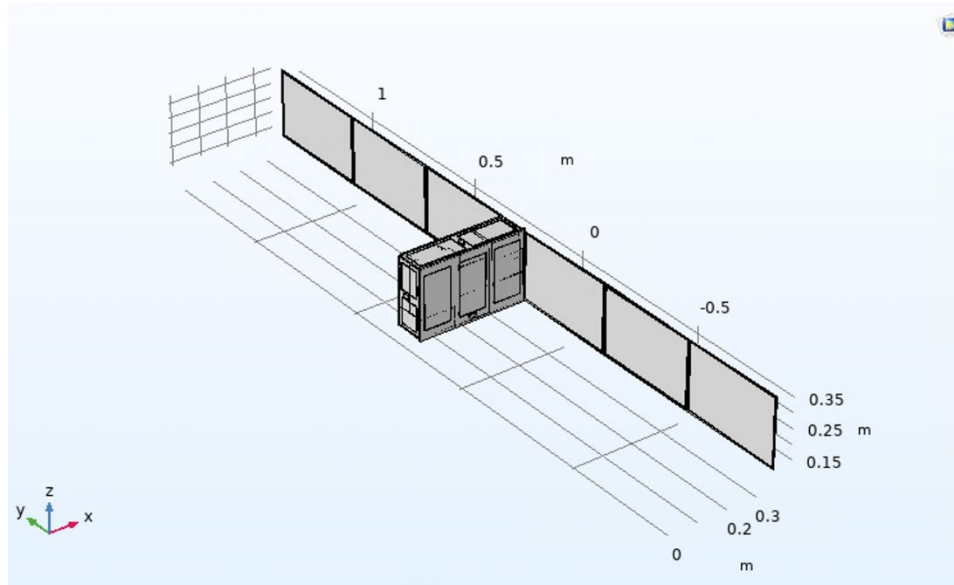


Figure 10: Defeatured COMSOL model of Appleton.

The COMSOL simulation was set up as a “Heat Transfer with Surface-to-Surface Radiation” model allowing for the analysis of the temperature across all components of Appleton. The body of the spacecraft was set as 7075 Aluminum (Al), the solar panels as Gallium Indium Phosphide (GaInP), and any open was covered by 0.5 mm of Aluminumized Mylar Film. The material properties for each of the materials used were taken from the COMSOL Multiphysics material library.

After entering the STK data into COMSOL, solar energy was modeled as a heat flux model. In order to account for the solar intensity and the solar vector, the heat flux model was defined by Equation 2, where  $SI(t)$  represents solar intensity over time, and  $SV(t)$  represents the solar vector component over time.

$$Q_o = S \cdot SI(t) \cdot SV(t) \quad (2)$$

Each component of the solar vector was set up to influence its respective side of Appleton. The blackbody radiation of Earth and the albedo of Earth were also modeled as heat flux models with both factors influencing the nadir side of Appleton. The albedo and blackbody radiation were modeled using constant values, corresponding to the average values discussed earlier. Each component in Appleton was modeled as a heat source within COMSOL, setting the value to the power dissipated by the component calculated earlier. The ambient temperature of space was set to be equal to  $-270.45\text{ }^{\circ}\text{C}$  (Bograd et al., 2018). Figures 11 and 12 below show the set up for the COMSOL model.

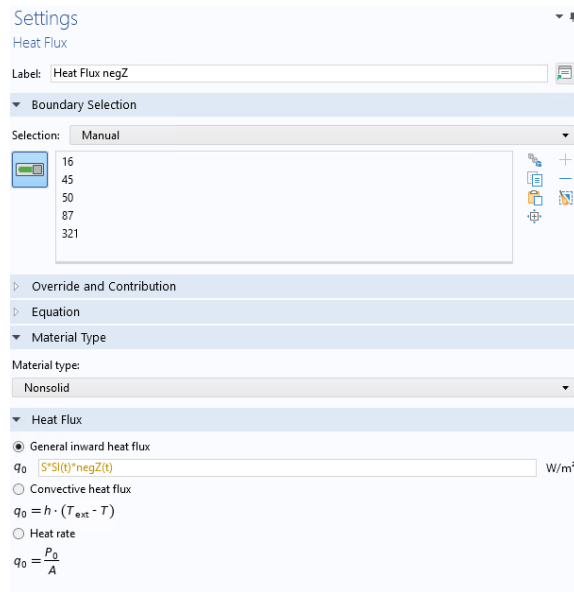


Figure 11: Set Up of COMSOL Heat Flux.

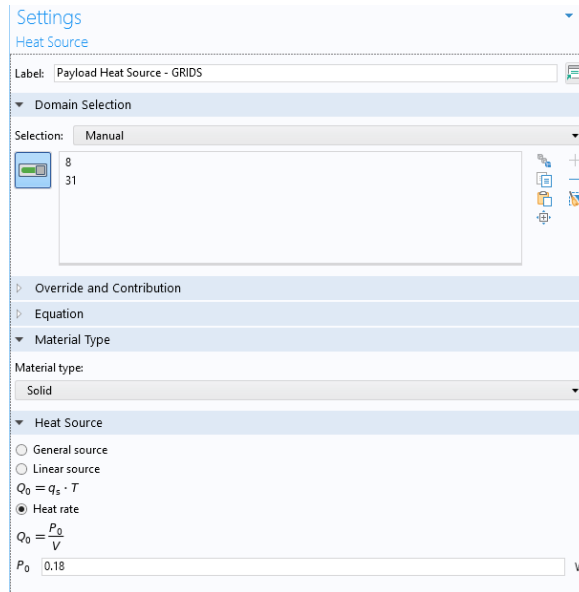


Figure 12: Set Up of COMSOL Heat Source.

### 3.3 Results, Discussion, and Design Considerations

The average surface temperature of Appleton was calculated over its orbit along with its solar vector and intensity data while in STK. The data from STK shows that Appleton will have an average temperature range of  $-20.8 - 22.6$  °C. The average temperature is plotted over 24 hours in Figure 13.

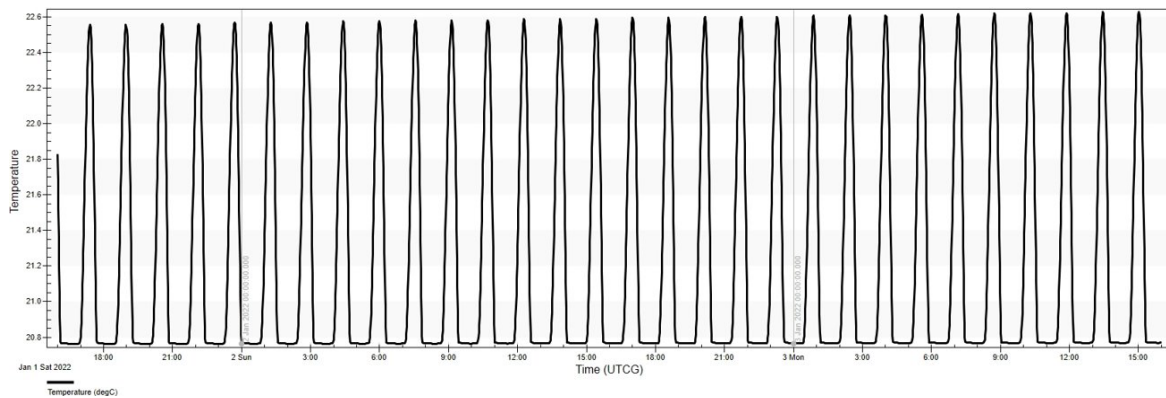


Figure 13: Appleton Average surface temperature (°C) over 24 hours from STK SEET simulation.

The temperature data derived from STK SEET however is limited in its nature. The SEET temperature data does not factor in the blackbody radiation of Earth, any internal heat generation,

and the body of the spacecraft model is limited to only be aluminum. Because of the limitations of STK the results must be compared to those from COMSOL. Figures 14 through 17 show the COMSOL thermal model of Appleton after one complete orbit. The maximum temperature of Appleton is 785 K, and the lowest is 235 K. Although surfaces on Appleton reach temperatures that are significantly outside of the thermal limit of  $-20 - 50\text{ }^{\circ}\text{C}$ , no components on the interior of Appleton reach these temperatures. Any hot point on Appleton is limited to the exterior of the satellite and the thermal insulation provided by the structure protects the components on the interior of Appleton. Throughout the duration of the mission, no internal components of Appleton exceed the thermal limit, thereby compromising the mission.

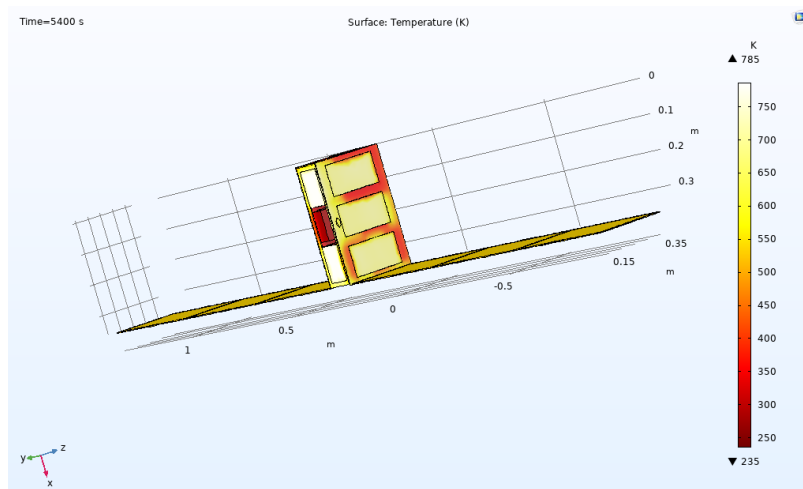


Figure 14: Appleton surface temperatures (K) from COMSOL with the Anti-Nadir (-Y) and Wake (-Z) showing.

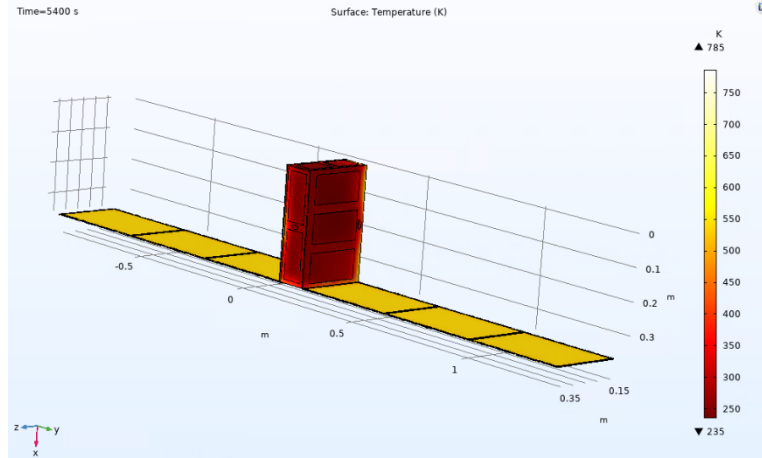


Figure 15: Appleton thermal analysis with Nadir (Y) and RAM (Z) sides showing.

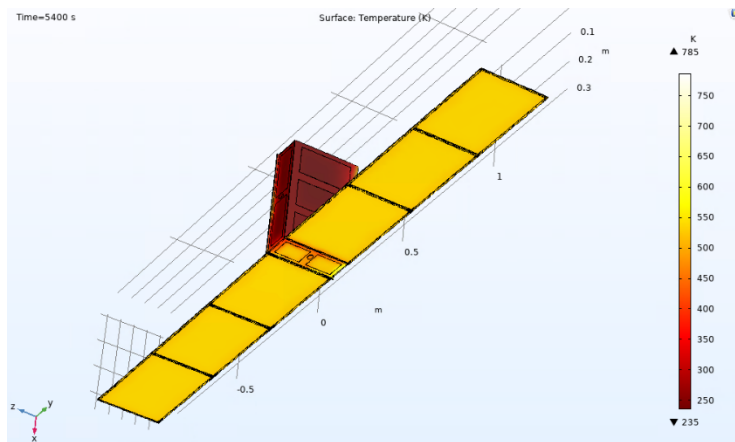


Figure 16: Appleton temperature from COMSOL with Sun Facing Side (X) showing.

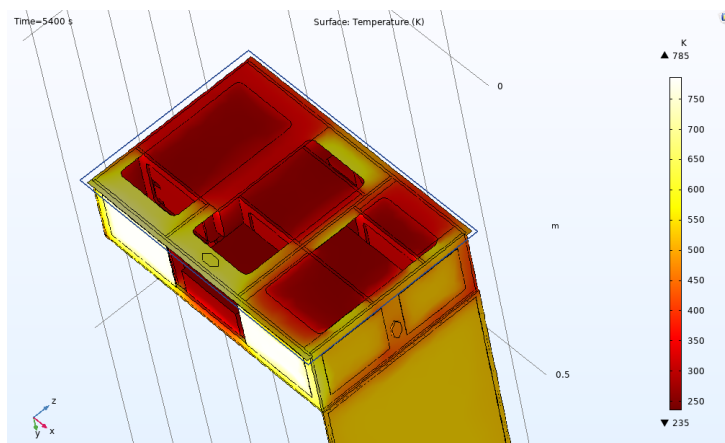


Figure 17: Appleton Thermal Analysis (Internals Exposed).

## **4. Analysis and Design Considerations for Space Plasma, Radiation and Debris Environment Interactions**

The space environment and its effects on space systems must be understood and evaluated for any space mission. Of particular concern are the effects present in the ionosphere. These include ambient electromagnetic and radiation environments as well as the potential for micrometeor or space debris impacts. The following section contains analysis of the risks posed by these phenomena and any effects experienced by Appleton over the course of its mission lifespan.

### **4.1 Ionosphere Overview**

Appleton's orbit places it in the ionosphere, the region of the Earth's atmosphere between altitudes of roughly 80 and 600 km. In this region extreme ultraviolet and x-ray solar radiation are present which ionize the trace gases present. The amount of incoming solar radiation flux varies depending on the solar cycle and can change up to a factor of ten (Space Weather Prediction Center). This ionizing effect results in a layer of electrons developing. Due to the presence of this layer, radio communication of certain frequencies coming from the Earth's surface can be reflected and travel longer ranges around the curvature of the Earth. The presence of the ionosphere in human knowledge does not appear until 1902 when Oliver Heaviside and Arthur Kennelly predicted its existence as a possible explanation for the enhanced travel distance of radio waves. In 1924 Edward Appleton and his team used Ionograms; recordings of reflected high frequency radio pulses, to measure the virtual height of different ionospheric layers (UCAR Center for Science and Education). Since this discovery, the ionosphere has been separated into several layers depending on the frequency of radio waves they reflect, with higher layers reflecting higher frequency waves than lower layers, as shown in Figure 18.

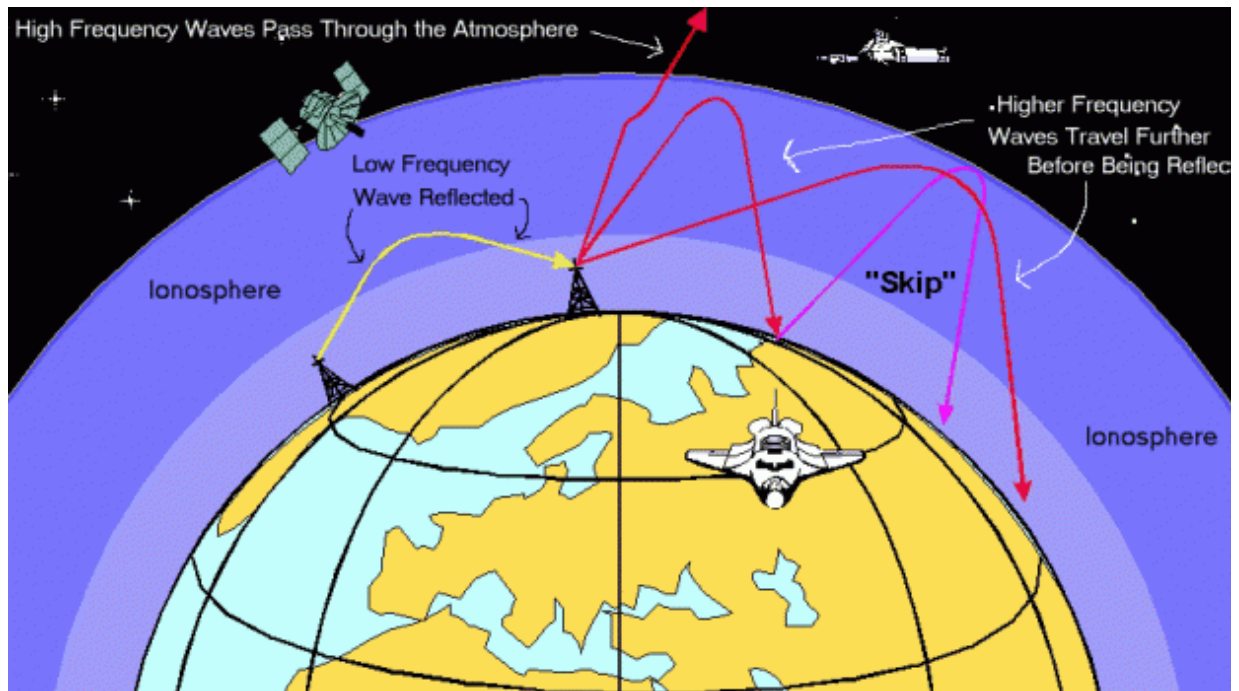


Figure 18: Interaction between the Ionosphere and Different Radio Wave Frequencies (Space Weather Prediction Center)

The ionosphere can be broken into three main layers: D, E, and F. The D Layer is the lowest and covers altitudes between ~70 to 80 km above sea level, occurring within the Mesosphere. The E layer occurs between 100 and 110 km above sea level, within the Thermosphere. At the highest altitude, the F layer occurs at the edge of the thermosphere and covers an altitude between 200 to 600 km. The locations of these layers are shown in Figure 19.

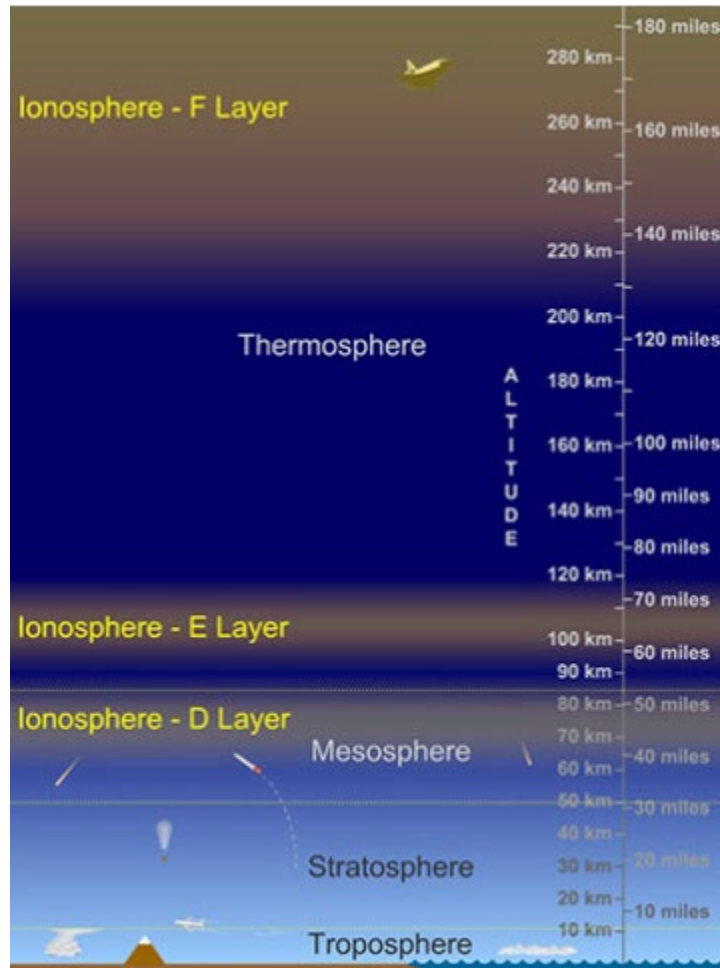


Figure 19: Layers of the Ionosphere and their altitudes relative to sea level (UCAR Center for Science and Education)

These regions vary depending on the level of solar activity. Some regions such as the D and E layer can even disappear entirely overnight due to the significant reduction of ionization when the sun is not present. This is a result of ions recombining with electrons to attain a neutral charge. But the highest region, the F layer, can remain even during the night. This is due to the level of ionization and rarity of gas species, which reduces the likelihood of recombination and allows the ionized species and electron layer to persist until solar activity increases again during the daytime (UCAR Center for Science and Education). The Appleton spacecraft will occupy an orbit that takes it across the entire altitude range of the F layer, allowing for the collection of data

regarding the local ion composition and state during different periods of the day and levels of solar activity. To prepare for this mission several effects on the spacecraft and potential risks due to this dynamic layer of the atmosphere must be modeled.

#### **4.2 Surface Charging Analysis and Design Considerations**

A trait characteristic of the ionosphere is the presence of plasma, an electrically conductive gas that consists of multiple ion species combined with free electrons. When the spacecraft interacts with these particles its surface becomes electrically charged and develops a potential. Due to high flux of electrons in comparison to ions, the spacecraft potential of a conducting surface will be negative. The potential may reach an equilibrium so that the flux of electron (repelled species) and ion (attracted species) are equal. In reality, spacecraft have conducting and dielectric surfaces and as such its surface potential may not reach equilibrium and is not uniform. Additional sources of charging include energetic particle streams and solar UV photons, which positively charge the spacecraft. Free electrons also participate in the process resulting in negative charging of the surface. Since electrons have much lower mass than the positively charged ions, they travel at higher speeds and are more likely to contact the spacecraft (Koontz, 2018). They also carry more charge than UV photons, meaning spacecraft surfaces trend toward a negative potential difference when compared to the surrounding particles. In addition to plasmas and particles from solar activity, the effect of auroral charged particles must be considered. These particles can measure on the order of 100 keV and carry much higher potential for damage. This is of particular concern as the Appleton CubeSat will occupy a polar orbit, and as such will be exposed to auroral activity. Other systems on-board the satellite, such as electrical power and propulsion systems, can also contribute to surface charge accumulation.

The hazard posed by this charging is the potential for electrical discharges. Such discharges

can lead to noise in avionics systems, failure of components or power systems, and severe damage to internal dielectrics or the scientific payload (Koontz, 2018). It is also possible for intense surface arcs to increase propellant use rates, as these arcs may eject material resulting in propulsive effects. An image of these effects is shown in Figure 20, where local plasma is interacting with spacecraft surface metals and dielectrics (Garrett and Whittlesey, 2012).

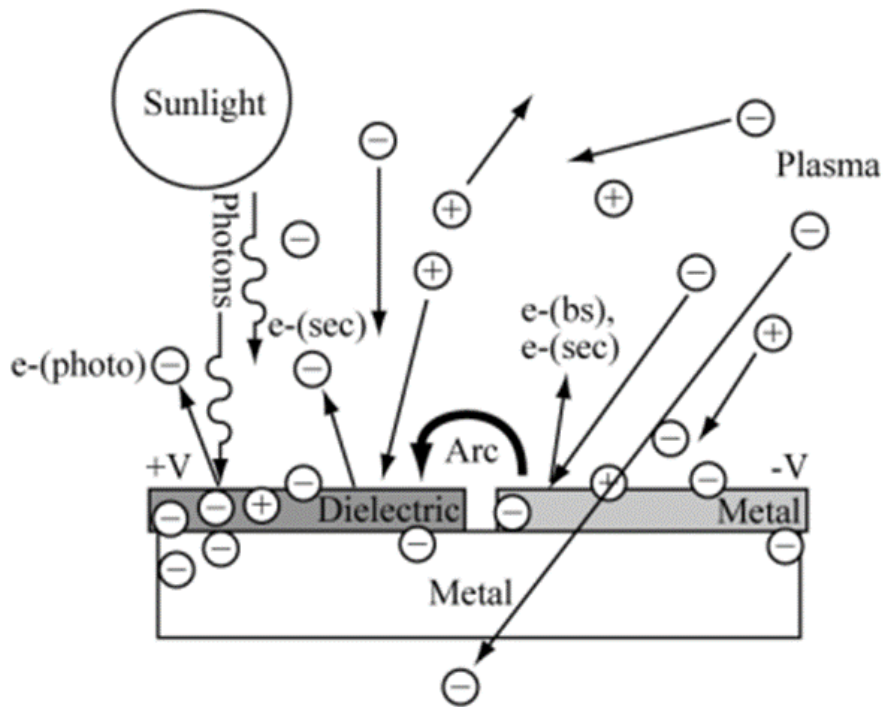


Figure 20: Plasma interactions with spacecraft surfaces (Garrett and Whittlesey, 2012).

There are two forms of surface charging, absolute and differential (Koontz, 2018). Absolute charging occurs from processes that result in an electrical potential or voltage difference between the surface of the spacecraft and the surrounding environment (Koontz, 2018). Differential charging occurs when two different sections of the spacecraft are isolated electrically and attain different levels of surface potential. When charging or discharging of these elements occurs there exists the potential for damage of spacecraft systems. As such it is necessary to model

these effects and ensure that the spacecraft is adequately insulated to absorb incoming energy, according to Figure 21, and does not have any components or exposed dielectrics that would allow for differential charging.

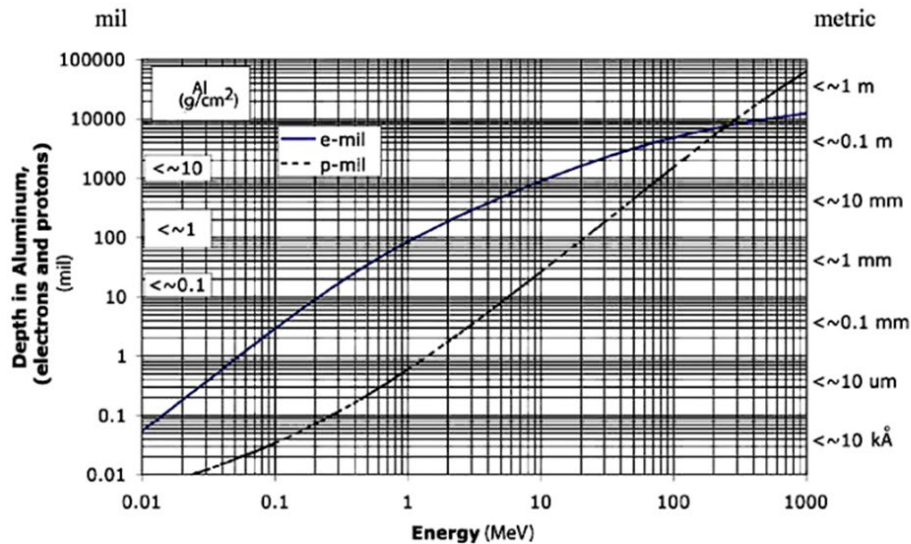


Figure 21: Thickness of Aluminum shielding capable of absorbing certain energy levels  
(Garrett and Whittlesey, 2012)

In order to simulate the effects of charging on the spacecraft the Space Plasma Interaction System (SPIS) was used. SPIS is an under-development European Space Agency (ESA) program which allows for the simulation of plasma effects on various spacecraft surfaces and components. The program requires a large set of parameters regarding the composition and state of local plasmas before it is able to run. Additionally, it requires legacy geometric models of any spacecraft using a program called Gmesh, and only will run with models using version 2.4.2 or earlier of the software. To begin setting up the charging simulation one must first collect information regarding the location of the spacecraft. This was done using STK to propagate the orbit and retrieve latitude, longitude, and altitude of the satellite at a particular location in its orbit. For this analysis the

location chosen was above the north pole, where the potential exists for aurora activity, which provided the parameters shown in Table 6.

Table 6: Positional Parameters of Appleton above the North Pole.

Latitude (deg)	82.151
Longitude (deg)	-122.487
Altitude (km)	505.212

From this positional data the local composition and state of the ionosphere at a specific date can be determined. The date chosen for this analysis was selected to coincide with a similar level of solar activity to the solar maximum Appleton will experience during its mission. Since Appleton would be launching at the beginning of solar cycle 25, the solar activity is going to gradually increase for the duration of the mission. By using solar activity data from solar cycle 24 it is possible to predict the level of activity Appleton will experience near the end of its scientific mission.



Figure 22: Solar Activity, measured by sunspots, across recent Solar Cycles

(SpaceWeatherLive.com, 2021)

As seen from Figure 22, similar solar conditions existed during the month of Sept. 2010. To retrieve ionospheric data from the previously selected date and position, an online atmospheric model was applied. In this case the International Reference Ionosphere (IRI) from the Community Coordinated Modeling Center (CCMC) was used (Rastaetter, 2016). Inputting the location data from Table 6 along with the date where similar solar activity was present allows for the computation of the following ionospheric parameters, shown in Table 7.

Table 7: IRI Outputs for Sept. 2010

Parameter	Value
Electron Density, $n_e$ ( $m^{-3}$ )	4.5E10
Neutral Species Temperature, $T_n$ (K)	826
Ion Species Temperature, $T_i$ (K)	1700
Electron Temperature, $T_e$ (K)	2580

O <sup>+</sup> ions (%)	92.1
H <sup>+</sup> ions (%)	3
He <sup>+</sup> ions (%)	0.7
N <sup>+</sup> ions (%)	4.3

The parameters in Table 7 were inputted into the SPIS simulation setup along with a simplified geometric model of the 6U CubeSat main bus.

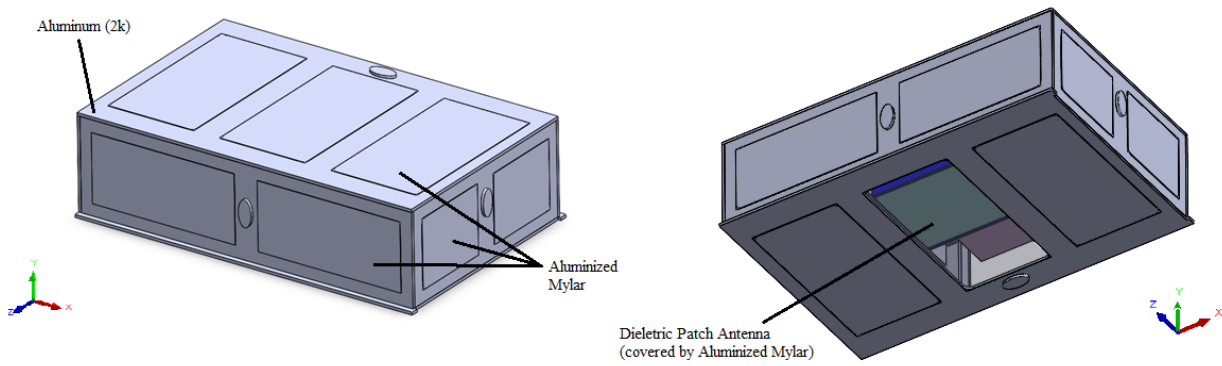


Figure 23: Surface materials of Appleton's 6U bus (excluding solar panels).

The surface properties of the aluminum chassis and aluminized Mylar as well as the dielectric patch antenna were specified in the simulation setup. The locations of these materials are shown in Figure 23.

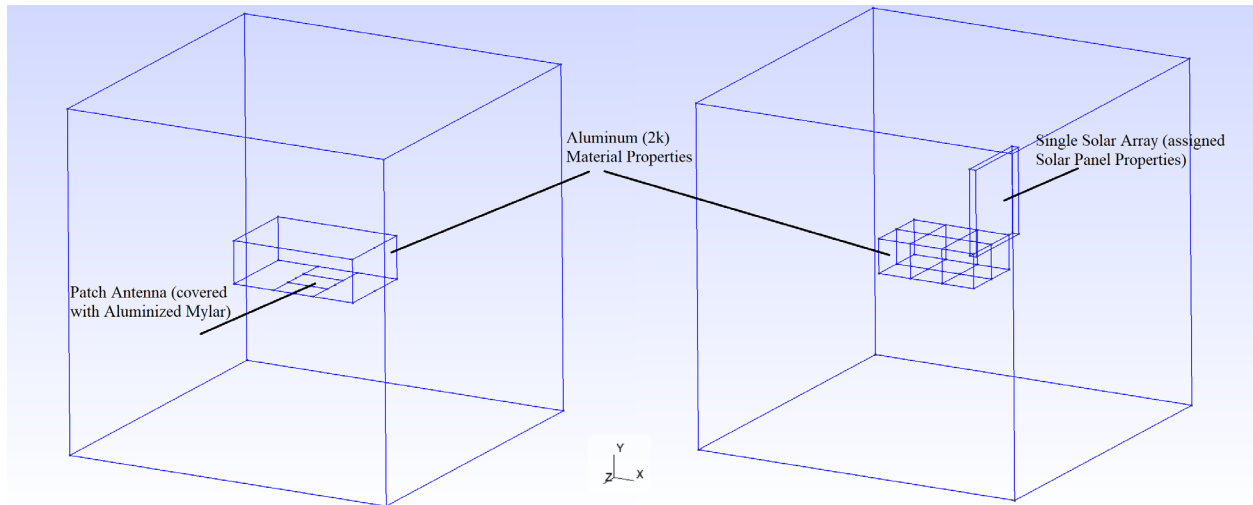


Figure 24: Simplified GMESH model of Appleton's 6U bus, excluding and including a single solar array panel

Two simulations were performed, one with only the 6U body and another with a single solar panel extended. This was done because SPIS has limitations with the number of surfaces which can be assigned properties, meaning the entire spacecraft was unable to be accurately simulated without further simplification. Fortunately, the main body of the spacecraft is fully conductive, and the dielectric patch antenna and solar panels have been properly grounded to the body. As such, it is expected that the CubeSat will charge evenly to the same potential difference relative to its surroundings. The models shown in Figure 24 were used in the SPIS simulation, with the surface properties shown.

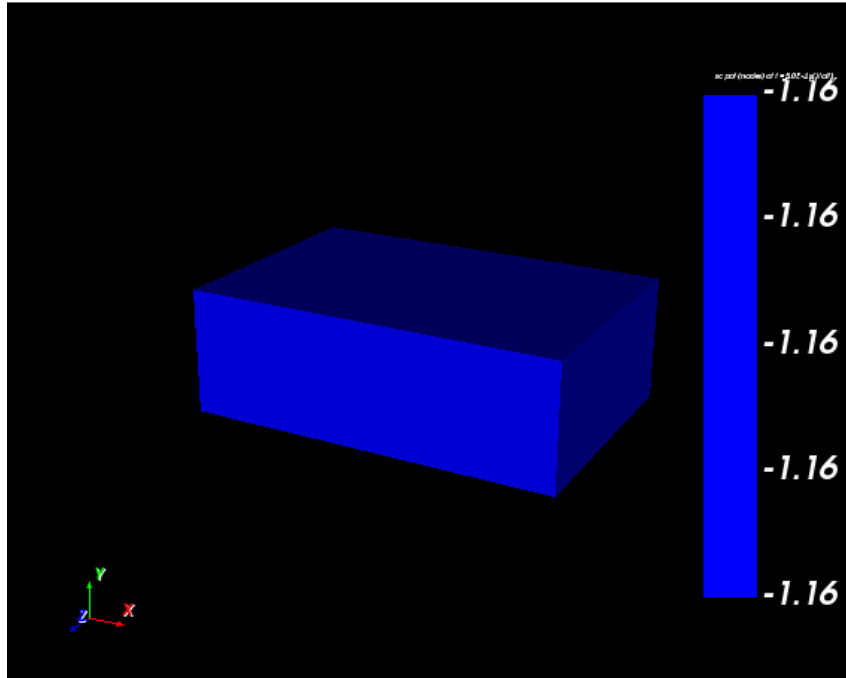


Figure 25: 6U CubeSat surface potentials (V) for fully conductive and grounded surface from SPIS.

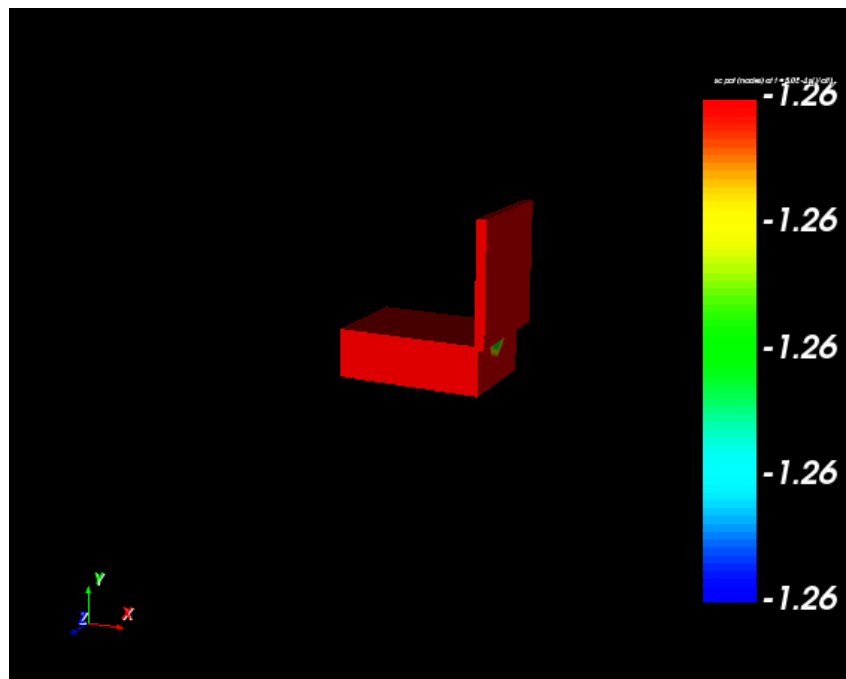


Figure 26: 6U CubeSat surface potentials (V) for fully conductive and grounded surface with a single solar array.

As seen in Figures 25 and 26 above, both simulations converged to negative potentials that were evenly distributed across the CubeSat surfaces. The floating potential in the first simulation converged to a value of -1.16 V, while the second simulation converged to -1.26 V. This is likely due to the increased surface area from the addition of the solar panel, as an increased area allows for more collisions between the CubeSat and the local plasma. Additionally, the charge is more negative due to the relatively high temperature of electrons compared to ions, as well as the fact that electrons in this plasma will have much greater thermal speed and thus random flux compared to that of the ions. From these results it is expected that should the entirety of Appleton be simulated, including fully deployed arrays, the negative potential would further increase. However, given that these values would be on the order of singular Volts it is unlikely that any significant damage would occur. If any damage did occur it would be located on the extended solar arrays, specifically within the power train leading back to the CubeSat battery. This is because the main body of the CubeSat is fully conductive while parts of the solar array contain materials of varying conductance. Since Appleton has a relatively short mission duration, it is not likely that significant damage would occur, and as such any protective anti-static coatings are deemed unnecessary. However, there still exists the possibility of mission critical systems failing due to aurora activity, and it is suggested that further investigation of aurora effects be the focus of future work.

### **4.3 Analysis of Induced Magnetic Fields Effects and Design Considerations**

Since the Appleton CubeSat will be carrying a magnetorquer for ADCS it is necessary to model the potential interactions this induced magnetic field will have on other spacecraft systems. Of particular concern will be the interaction between this field and the scientific payload, as well as any magnetometers being used for ADCS. Additionally, it will be necessary for ground testing of the ADCS system that accurate models of the ambient geomagnetic field are created. The

strengths of these fields must be ascertained, as high field intensity within the spacecraft may lead to damaging of equipment, corruption of on-board data, prevention of data collection or transmission, erroneous data from the payload, or incorrect information regarding the spacecraft attitude.

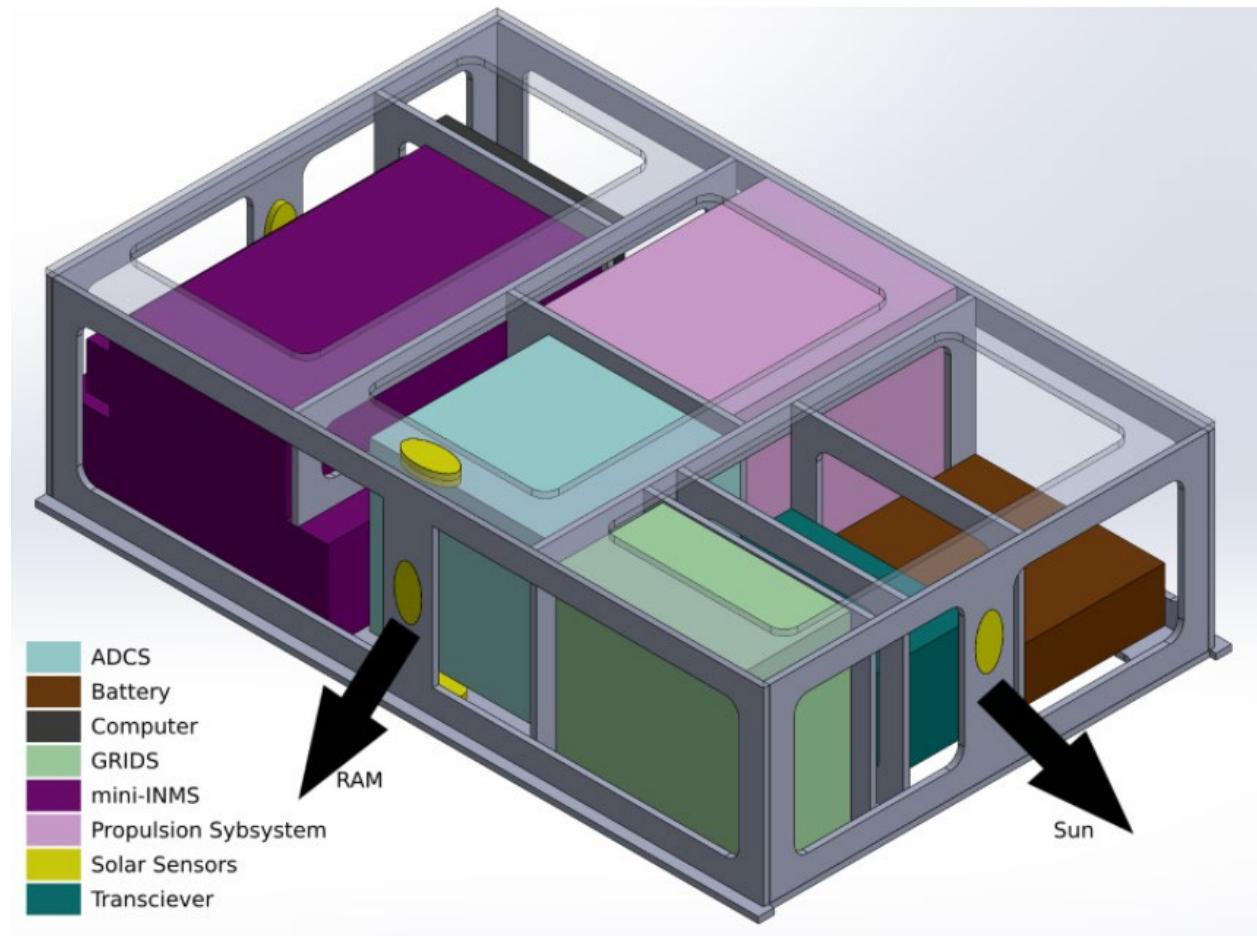


Figure 27: The location of Appleton’s primary systems. In the ADCS block, the magnetorquer is located at the geometric center of the CubeSat.

To assess the strength of internal magnetic fields resulting from the on-board magnetorquers a COMSOL model was developed. The magnetorquer board selected for this mission is the ISIS CubeSat MagneTorQuer board (iMTQ), which can produce a maximum torque of  $0.2 \text{ Am}^2$ . To simplify the model, a single magnetorquer rod was considered located at the

geometric center of the CubeSat, contained within the ADCS block shown in Figure 27. The model was then considered as 2D by assuming radial symmetry of the resulting magnetic fields. As such, the magnetorquer could be treated as a permanent bar magnet with a field strength corresponding to the highest duty cycle torque it can produce. The remanent field was calculated from the 0.2 Am<sup>2</sup> torque to be 0.04267 Tesla by:

$$m = \frac{1}{\mu_0} B_r V \quad (3)$$

Where  $m$  is the torque of 0.2 Am<sup>2</sup>,  $\mu_0 = 4\pi \times 10e - 7$  H/m,  $V$  is the volume of the magnet, and  $B_r$  is the remanent field strength. Inputting these material properties into a COMSOL physics simulation produced a plot of the magnetic flux density within the CubeSat, shown in Figure 28.

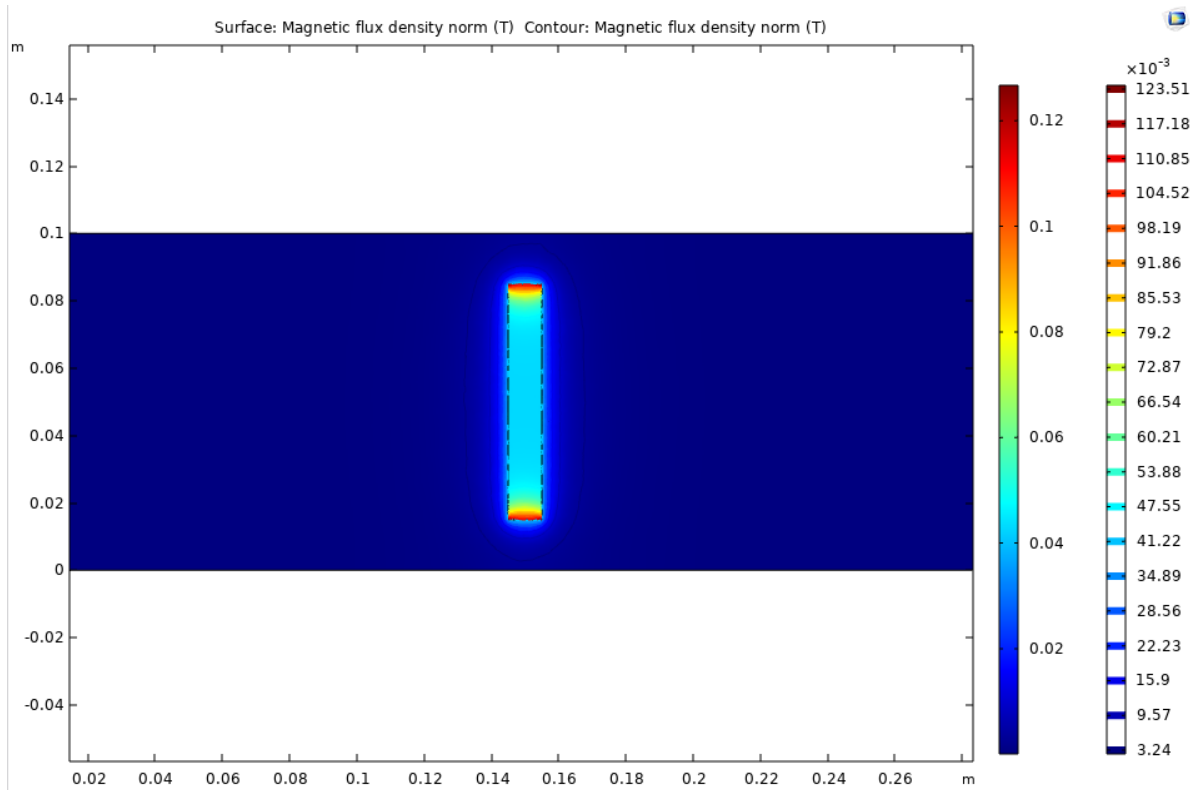


Figure 28: Magnetic flux density (Tesla) within the 6U CubeSat induced by the operation of a magnetorquer from COMSOL simulation.

The strength of the magnetic field is shown to decrease substantially as the distance from

the magnetorquer increases. As seen in Figure 28, magnetic flux reaches a value of  $3.24 \times 10^{-3}$  Tesla at 1.5 cm from the magnetorquer. At these levels the magnetic field is still significant enough to have an impact on the recordings of on-board magnetometers. However, the ISIS CubeSat MagneTorQuer board chosen for this mission contains a built-in magnetometer on the board, which likely has been calibrated to account for the influence of the generated fields. Information regarding the calibration is unavailable from the supplier, and if such a calibration was not included then external magnetometers should be considered.

#### **4.4 Analysis of Radiation Effects and Design Considerations**

Ambient radiation is another environmental effect that has a degrading effect on systems overtime. Of concern for the Appleton design are effects from protons and electrons trapped within the Van Allen belts, heavy ions within the magnetosphere, cosmic rays containing protons or heavy ions, and protons or ions released during solar flares (O'Bryan, 1998). Electronic devices are susceptible to long term damage due to these effects, especially from high energy electrons and protons. Device shielding from the aluminum body of the spacecraft can effectively attenuate high energy electrons but falls short in preventing high energy protons ( $>30$  MeV) from damaging components. If single particles do contact a component, then what occurs is referred to as a Single Event Effect (SEE) (O'Bryan, 2015). There are two types of SEEs which are galactic cosmic rays (GCRs), specifically their heavy ion component, and high energy protons. These events do not usually pose significant danger to systems but may results in transient pulses within circuitry, or corruption of bits in the on-board memory storage (O'Bryan, 2015). However, it is also possible that serious errors can occur, called single event upsets, which can interact with finer electronics on devices resulting in frozen bits, or Gate Rupture (when the conductive path on a PCB is destroyed) which can completely disable critical systems. To determine the risk posed by these

interactions, the Total Ionizing Dose (TID) must be considered (O’Bryan, 2021).

To ensure that the TID will not cause damage to core components of Appleton, the accumulated dosage must be compared to the radiation tolerances of the individual components, which have a minimum radiation tolerance of 2 krad. Most components, however, have tolerances on the order of 10 krad with the exact value specified by the manufacturer.

To measure the accumulated radiation dose for the mission duration, STK: SEET was utilized. Flux models based on NASA’s AE-8 radiation belt maps for electron flux and AP-8 radiation belt maps for proton flux were implemented into the simulation (AGI, 2020). The radiation was measured behind 118.2 Mils and 19.7 Mils of aluminum, which represent the thickness of Appleton’s aluminum chassis and aluminized mylar respectively. These parameters were applied to the scientific orbit of Appleton and used to calculate the estimated TID for the mission duration.

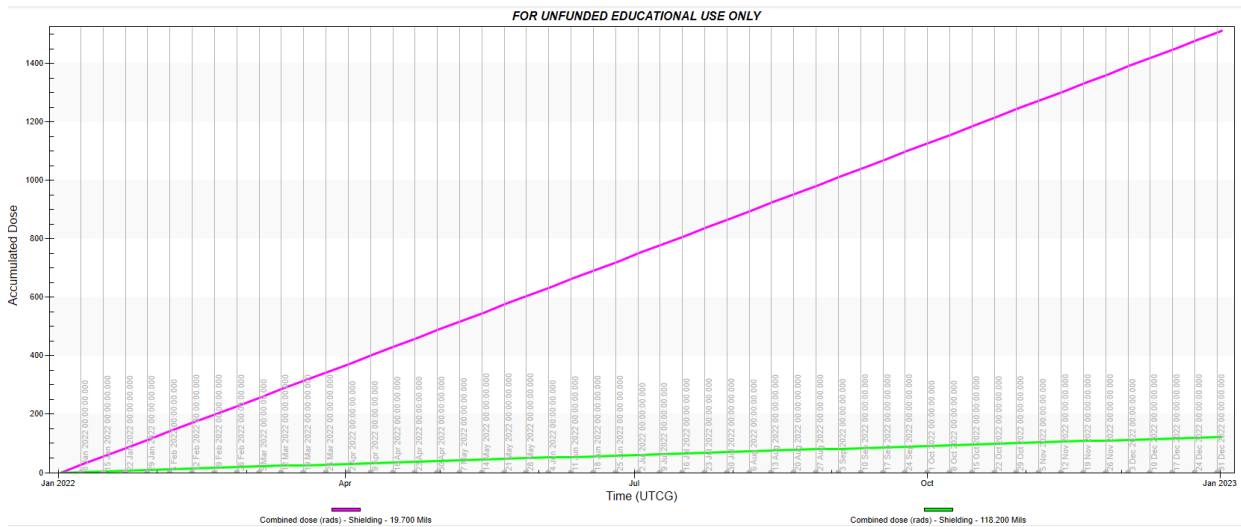


Figure 29: Accumulated Radiation Dosage or Total Ionizing Dosage (TID) over Appleton’s scientific mission duration from STK: SEET radiation simulation.

As shown in Figure 29, the TID amounts to a maximum of 1.5 krad for the case of 19.7

Mils aluminized mylar, and a minimum of 122 rad for the case of 118.2 Mils aluminum. Taking the higher of these two values as the worst-case accumulated dosage, it remains below the typical radiation tolerance of each CubeSat component (2 krad). In the case of the solar array, the degradation due to radiation is accounted for by the manufacturer, and its tolerance is given in the number of years before failure rather than an explicit rad value. It should be noted that the TID would eventually increase to a level exceeding internal component radiation tolerance for an extended mission duration. However, due to the relatively short mission lifetime of Appleton, radiation levels remain within acceptable parameters thus requiring no additional radiation shielding.

STK's SEET add-on was also used for determining the flux of GCRs at various energy levels. The Badhwar-O'Neill 2010 model includes measurements of GCR flux from 1955 to 2010, across solar cycles 19 to 24 (AGI, 2020). Measurements are based on NASA's Advanced Composition Explorer (ACE) Cosmic Ray Isotope Spectrometer (CRIS). Since the majority of GCRs are hydrogen protons (90%) these were the primary particles analyzed. Most of the CubeSat will be protected from these cosmic rays by the aluminum and aluminized Mylar, but solar cells are susceptible to penetration by high energy protons with energy levels of at least 4.2 MeV (Adams, 2008). The solar influence on the simulation was set to "Solar Max" to account for the worst-case scenario of the sun's contribution to these cosmic rays.

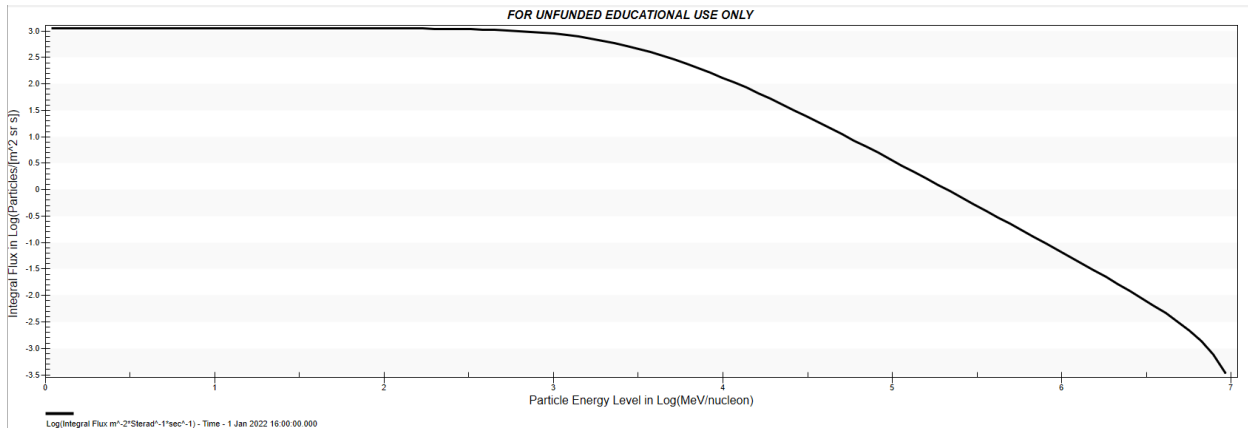


Figure 30: Integral Flux of hydrogen protons vs. energy levels over the Appleton mission duration from STK: SEET GCR simulation.

As shown in Figure 30, there exists a non-negative flux above 4.2 MeV, which suggests that Appleton’s solar panels will be susceptible to penetration by this form of radiation. However, it is assumed that these radiation effects are also accounted for in the solar cells advertised lifetime and would not cause significant damage over the mission duration. The only case which would lead to catastrophic effects would be for a large flux of higher energy protons, or heavier GCRs such as Iron, to impact the CubeSat. But this is unlikely as the mission operates within the magnetosphere and thus most high energy particles are blocked from reaching orbits as low as Appleton’s.

Another cause for concern is Solar Energetic Particles (SEPs) which are protons and ions carried by the solar wind. SEP levels correspond to the amount of solar activity coming from the sun, and so will increase as the solar cycle approaches its peak and decrease as it approaches solar minimum. Since Appleton is launching at the start of solar cycle 25, the risk posed by SEPs will start off as minimal and increase over the duration of the mission. The model used in STK: SEET is the ESP model. The ESP model includes data from three complete solar cycles (20-22) of proton observations with predictions being made for energies between 1 MeV to over 100 MeV. This

model also includes a formulation of the worst case fluence expected (AGI, 2020).

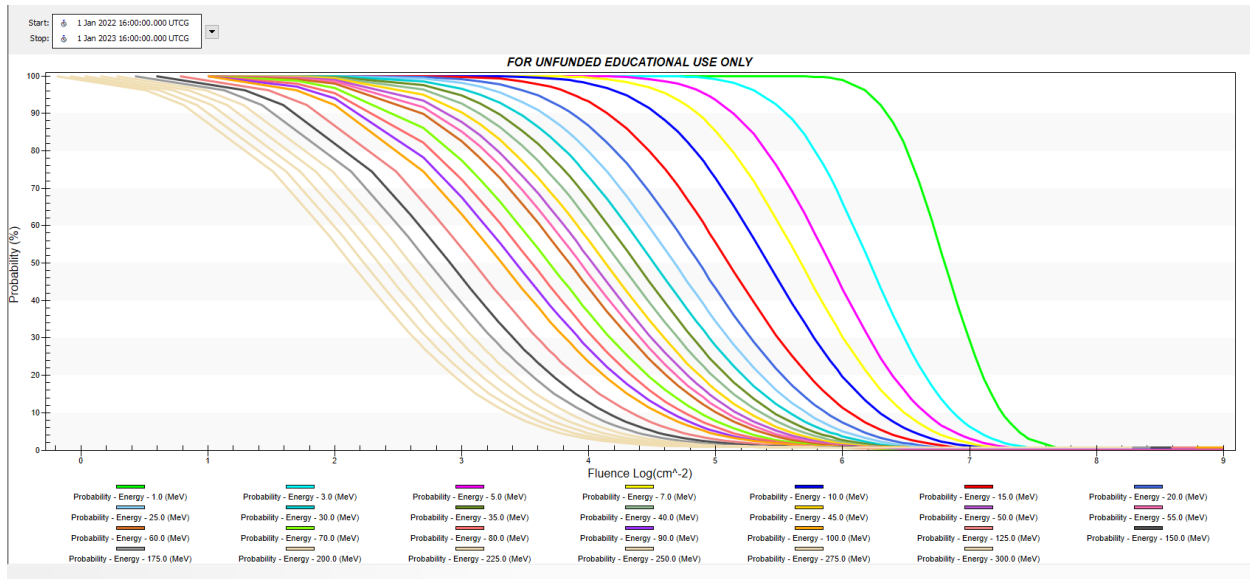


Figure 31: SEP Probability vs Fluence level over the Appleton mission duration from STK: SEET SEP simulation.

As seen in Figure 31, the probability of SEPs effecting Appleton is 100%. However, it can be observed that the probability of high energy, and therefore damaging, SEPs rapidly decreases for higher fluence levels. These particles are still capable of damaging Appleton’s internal electronics; however, aluminum shielding can block most dangerous particles. Additionally, having a mission duration of 1 year further decreases the probability of damaging fluence being experienced as shown in Figure 32.

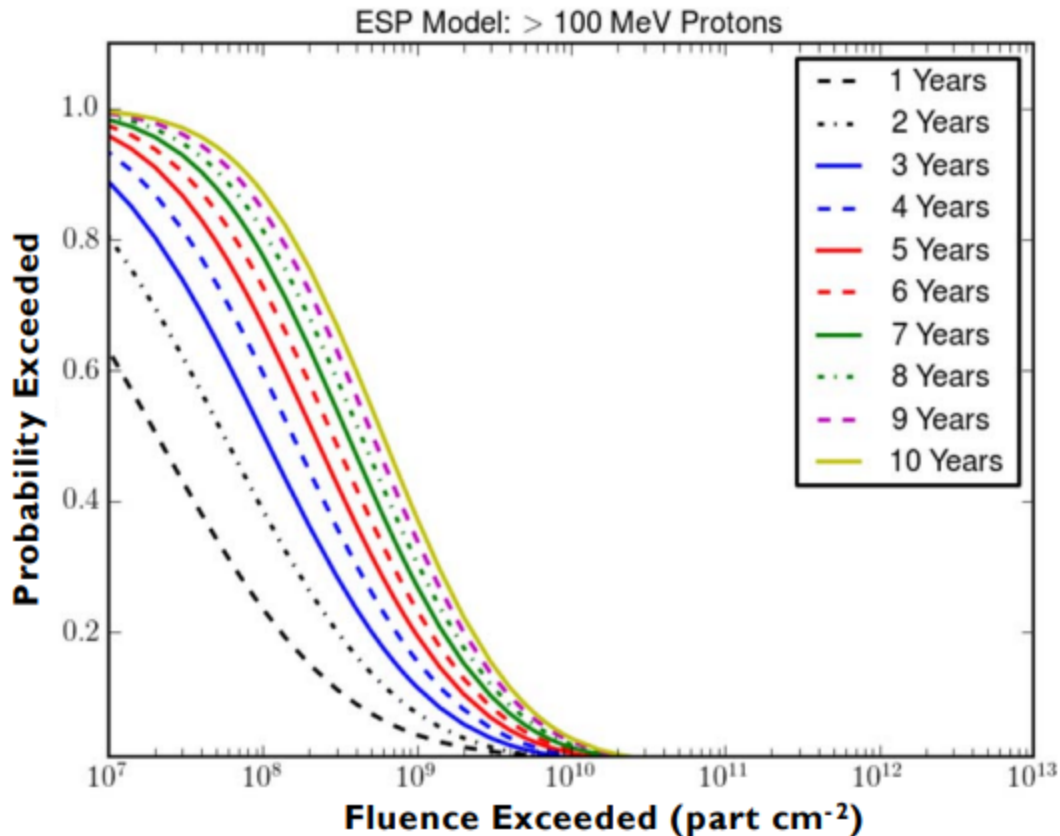


Figure 32: SEP Probability vs Fluence for various mission durations (AGI, 2020).

A low mission duration results in an ever-decreasing probability of SEP fluence exceeding 100 MeV (AGI, 2020). Therefore, it is expected that Appleton will have low risk from SEPs during its mission duration, and no additional shielding is necessary.

#### 4.5 Analysis of Micrometeorite and Space Debris Effects and Design Considerations

The orbital environment of Earth contains several man-made and naturally occurring particulates. These objects are typically on the order of 1  $\mu\text{g}$  to 10 mg in mass but travel at orbital velocities ( $>13$  km/s). Impacts from these particles therefore transfer a significant amount of energy when they collide with spacecraft, mostly in the form of thermal energy. Despite the extreme speeds these particles are travelling at, their size and mass result in minimal damage to spacecraft systems. While most space debris and micrometeors will not pose a threat to Appleton,

there is the possibility that an impact with a larger object may occur. Of particular concern would be impacts with the deployable solar array, as this array has less material protecting it from damage even from minor impacts. Overtime the environment degrades the performance of these systems until they are no longer functional.

To ensure Appleton remains functional for its mission duration, it is necessary to model the probability and scale of impacts as a function of time spent in the orbital environment. This was done using STK’s SEET tool which contains a space weather database accounting for meteor and particle debris in Earth’s orbit. The model used for this analysis is based on Kessler’s equations (1989), and it calculates the amount of the small orbital debris particle flux at a given time as a function of particle size, satellite average altitude, orbital inclination, and the average of the F10.7 solar activity index for the previous 13 months (AGI, 2020). The cross-sectional area used as the target for potential impacts was defined as the 3Ux2U face of the CubeSat’s main body, resulting in a target of 0.12 m<sup>2</sup>. Two analyses were performed, one where the target was pure aluminum and the other where the target was mylar. Additionally, damaging impacts are defined as any particulate which penetrates more than 0.5mm into the aluminum chassis of Appleton or into the aluminized mylar.

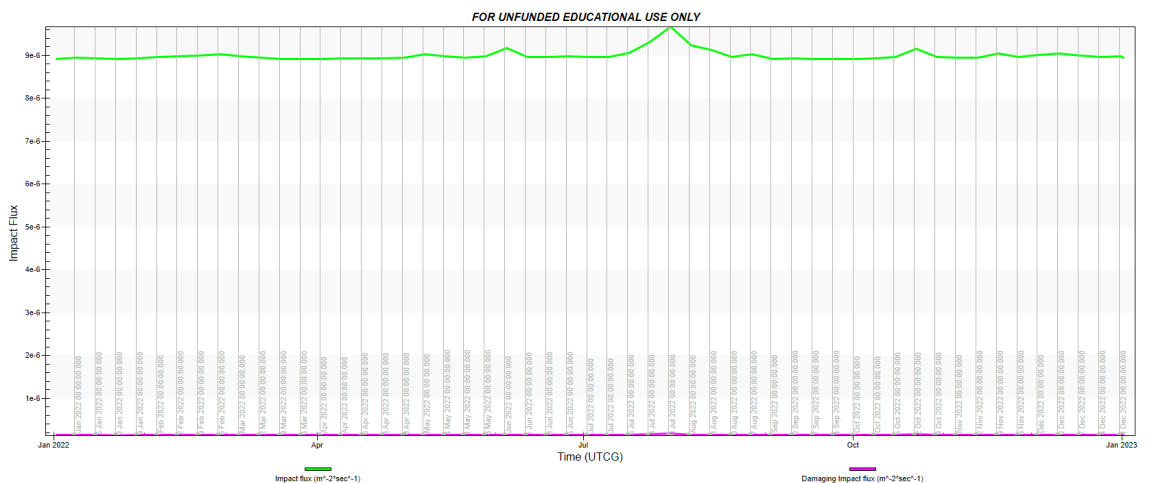


Figure 33: Impact Flux and Damaging Flux over the mission duration for an Aluminum target.

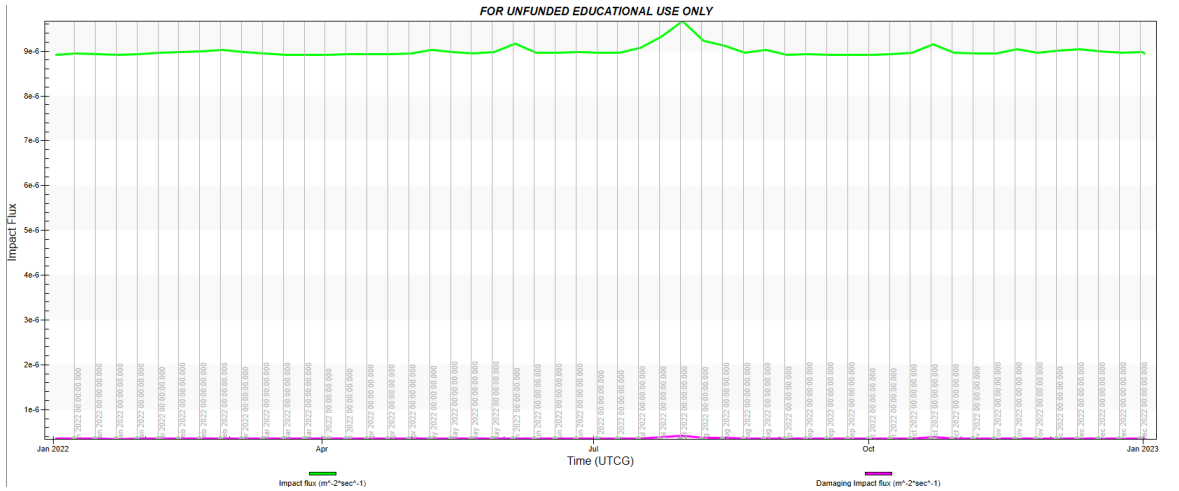


Figure 34: Impact Flux and Damaging Flux over the Appleton mission duration for a Mylar target from STK: SEET particle simulations.

As shown in Figures 33 and 34, the impact flux experienced by Appleton over the mission duration remains the same, with a peak occurring during an apparent meteor shown around the end of July 2022. This time also corresponds to the highest potentially damaging flux experienced by the CubeSat.

Table 8: Maximum Impact and Mass Flux for Space Particulates over the mission duration.

Damaging Impact Flux ( $m^{-2}*s^{-1}$ )	Damaging Impact Mass Flux ( $kg* m^{-2}*s^{-1}$ )	Impact Flux ( $m^{-2}*s^{-1}$ )	Impact Mass Flux ( $m^{-2}*s^{-1}$ )
3.5E-07	1.8E-16	9E-06	2.25E-16

Overall, the impact flux levels remained on the order of magnitude shown in Table 8 and are not likely to cause serious damage to Appleton over the mission duration. As such, there is no additional shielding necessary.

## 5. Helmholtz Cage

This section presents the current design and plans for the development of a functional Helmholtz cage to be used in ground tests of the ADCS. The method for magnetic field generation using the current design and the addition of potential air bearing platforms is discussed.

### 5.1 Review of Previous Work

A Helmholtz cage is the invention of German scientist and philosopher Hermann von Helmholtz (1821-1894). The cage consists of a pair of coils parallel to one another with each coil containing several windings. By running a current through these coil pairs, a magnetic field is created and amplified by the coil pair at the midpoint between them. The current Helmholtz cage structure and design is based on the design presented by Brown et al. (2021). The cage is made of three orthogonal coil pairs, mounted such that each pair can generate a magnetic field along a certain axis. The coil pairs are square and measure 1.44 m in length, the apparatus is shown in Figure 35. The manual for the assembly of the Helmholtz cage is in Appendix B.

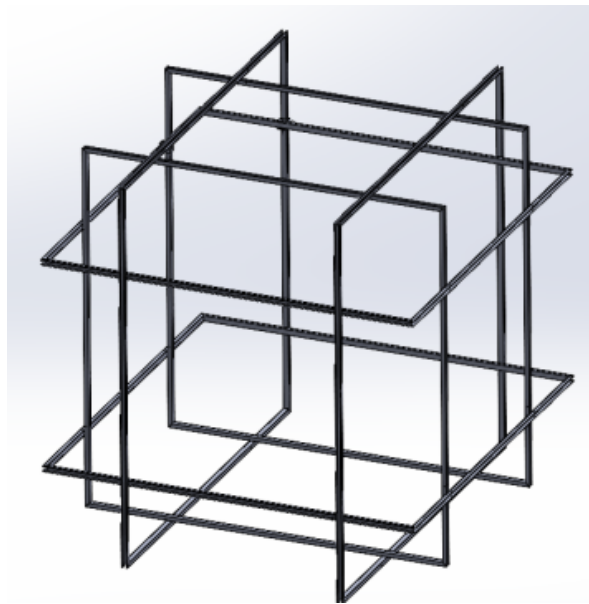


Figure 35: Helmholtz cage design (Brown et al., 2021)

To simulate the magnetic environment of the CubeSat it was required that the magnetic field remains within 1% of the required field strength, within a  $0.25 \text{ m}^3$  volume at the center of the cage. The strength of the magnetic field across this volume was predicted using the Biot-Savart law,

$$\bar{B} = \frac{\mu_0 n I}{4\pi} \int \frac{d\bar{I} \times \hat{r}}{r^2} \quad (4)$$

Where,  $\bar{B}$ , is the magnetic flux density,  $\mu_0$  is the permeability of free space,  $d\bar{I}$  is a wire element and  $\hat{r}$  is the unit vector of the distance between the wire element and a point within the magnetic field. Using this law, Brown et al (2021) was able to create a 2-dimensional plot showing the magnetic field strength relative to the desired value along the centerline of a single coil pair, as shown in Figure 36.

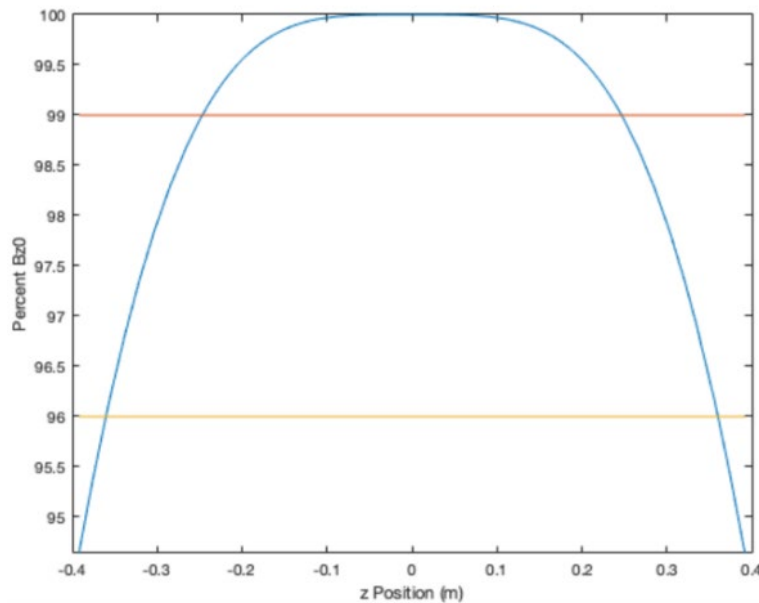


Figure 36: Helmholtz magnetic field strength along the centerline for a single coil pair (Brown et al., 2021)

After the construction of the cage a validation of the magnetic generation capabilities was necessary. To do this Brwon et al (2021) used Cytron 30A, 5-30 V Single Brushed DC Motor Controllers connected to the coil pairs on each axis to vary voltage, and hence the current, thereby controlling the magnetic field produced by the coils. An Adafruit's LIS3MDL triple-axis magnetometer was attached to a test bed at the center of the  $0.25 \text{ m}^3$  test volume to measure field strength at the center-point. This magnetometer can measure magnetic fields from  $\pm 4 \text{ G}$  to  $\pm 16 \text{ G}$ , at data rates from 155 Hz to 1000 Hz, allowing for real-time analysis of the cage's performance. Adafruit's INA260 sensor was used to monitor the current in the magnetic coils. This sensor measures current, voltage, and power use on the high or low side, and can measure up to 36V and 15A. An Arduino MEGA 2560 was used for data acquisition and required altering of I2C addresses to prevent erroneous data being sent. This requirement was necessary due to several identical magnetometers being used. A basic procedural outline is shown below:

- Sensor readings were plotted via Python Code
- Magnetic field data for the orbit was imported from STK as a .csv file

#### Test Procedure:

- Power supplied directly to DC motor controllers. The controllers are varied to achieve the current corresponding to the desired magnetic field strength, related via the Biot-Savart law.
- Current through the coils is monitored via the INA260 sensor.
- Magnetometer data is received by the Data Acquisition unit DAQ (Arduino MEGA 2560) and plotted via python code over the test duration.

- The resulting plot is then superimposed over a plot of the desired magnetic field to show the strength achieved relative to the desired.
  - Note that the magnetometer only measures field strength at a SINGLE point within the cage

The program was run for approximately 50 minutes of the 60 total minutes of data. To ensure the magnetic field generation and measurements were not affected, the cage structure was not touched during the testing process. Following the completion of the test, the collected magnetic field data were plotted against the desired field data as shown below in Figure 37:

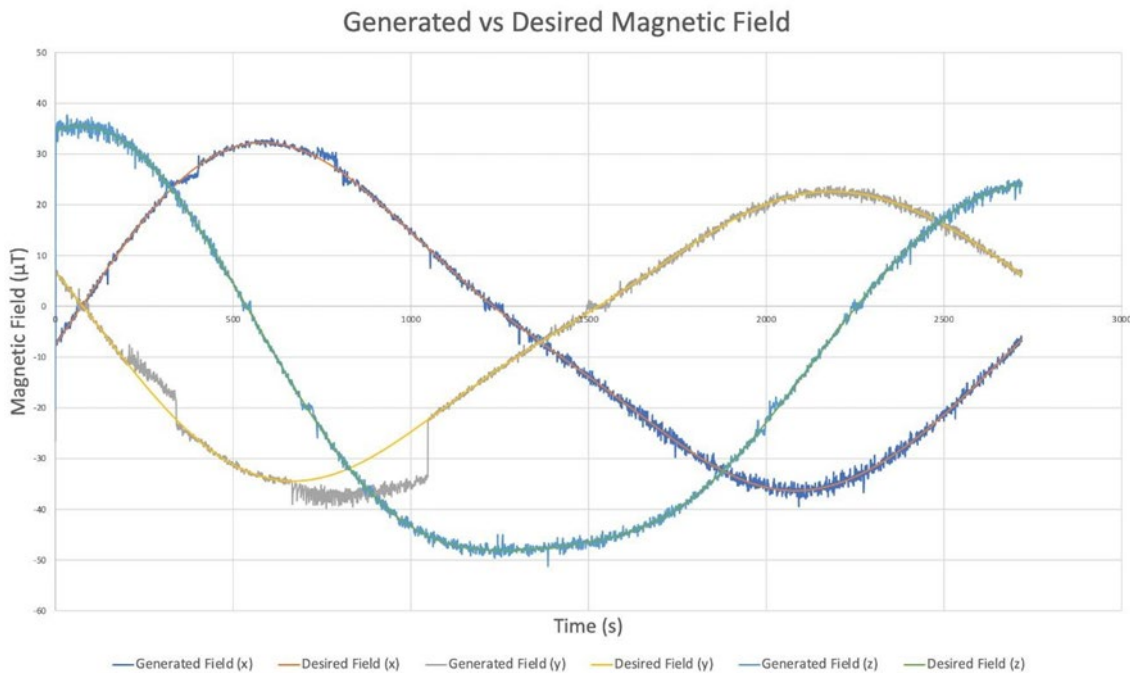


Figure 37: Helmholtz cage magnetic field test (Brown et al., 2021)

The data acquisition along the y-axis had the most significant discrepancy. The cause of these errors was not fully understood but was believed to be fully induced by errors in the setup of the Arduino control scheme (Brown et al., 2021). To improve the design, this year’s Appleton Project

Team decided to move the data acquisition into a LabView based control scheme using a LabJack as a replacement for the Arduino.

## **5.2 Updating the DAQ**

The software of the previous DAQ had limitations for the number of sensors that could be connected and was not in a centralized location. The Arduino script was responsible for collection and recording of data, while the Python script graphed the data. One issue identified was how the two scripts interacted with each other. An Arduino unit using the Inter-Integrated Circuit (I2C) interface was connected to the Inertial Measurement Unit (IMU.) This Arduino unit took measurements from the IMU, before passing data to the computer, where it was logged. Upon being logged by the Arduino program running on the computer, it would then be passed to a simultaneously running Python script to be graphed. This approach caused a problem for the recording of data, specifically, in terms of how it was passed. The Arduino code running on the computer expected data from the IMU to be passed at a certain data rate. However, data was not always being passed when it was expected, likely due to clock stretching and the maximum rate of data transfer from the IMU to the Arduino, and then from the Arduino to the computer. This led to the second problem of data not being passed correctly to the Python code. Data had to be passed to the Python script at regular intervals, upwards of 10 times per second for the graph to be helpful. However, the Python code could only read the data being passed to it at a set rate. This meant that if data were being passed too quickly it would begin skipping, resulting in occasional unrealistic numbers, or numbers including two decimal places.

Our team was able to resolve the issue of the mismatching data rates by slowing down the rate at which data was recorded from the IMU to the Arduino. However, one of our objectives was to integrate six additional three-axis magnetometers into the device to ensure that a uniform field

strength has been achieved. Unless only a couple of readings were taken per second, it would be impossible for the existing interface to handle quadrupling the rate of data throughout, which would result in an unacceptably low resolution.

Therefore, we replaced the existing DAQ with a more conventional design to resolve the problems of data resolution resulting from the simultaneous scripts. A LabJack U3 was selected as the replacement for the Arduino due to its ability to interface with LABVIEW and be expanded to include more sensor connections. In LABVIEW it is possible to centralize the processes that were previously written in separate locations (the Arduino and Python scripts). It is also a more convenient program to use for future updates to the Helmholtz cage DAQ as it is an industry standard and with further funding the LabJack U3 could be replaced with a more compatible National Instruments DAQ. With all sensors connected directly to the LabJack U3 and the LabJack connected to a computer with LABVIEW, the flow of data and its interpretation is more streamlined and concentrated in a single location. To further improve the DAQ it was decided that programmable power supplies should replace the existing DC power units. The current going through the Helmholtz coils can then be controlled in the same LABVIEW environment and script.

### **5.3 Updating Power Supplies**

The Brown et al (2021) project selected the Kungber variable DC power supplies to deliver power to the Helmholtz cage). Three separate power supplies were used, one power supply for each of the three pair of coils. To vary the current in each coil pair, the team used DC motor controllers. As part of the decision to integrate the Helmholtz cage into LabView, the team decided to upgrade the power supplies to the Unisource PSP-3010 Programmable DC Power Supply. The decision to upgrade the power supplies was made to remove the need for the DC motor controllers to manually change the voltage. The Unisource PSU allows the power supplies to be controlled

via LabView. By integrating the PSU into LabView it will allow for a more seamless and direct control option for adjusting the coil current and therefore the coils' magnetic fields.

#### **5.4 The I2C interface**

The 3-axis magnetometers use the Inter-Integrated Circuit (I2C) interface. This means they possess a clock and data pin to transmit data to the DAQ. The lab jack is not set up natively to interpret I2C, so code will either need to be found or created to do that. Additionally, each I2C device has an in-built address defined by the hardware of the device. To bypass the inability to use more than one of any sensors, a multiplexer was purchased with the intent of it being used to connect all of the magnetometers. This multiplexer accepts inputs from several I2C devices, and then assigns them all different I2C addresses. This multiplexer should then be connected to the LabJack.

Another possibility that we explored was not using 3-axis magnetometers but instead using single axis voltage varying magnetometers. These will change their voltage depending on the strength of the magnetic field, allowing them to be directly connected to the LabJack using analog input pins. However, this is suboptimal as each magnetometer needs its own input pin on the LabJack and provides less data than its I2C counterpart.

## **6. Conclusions, Recommendations, and Social Impacts**

The work completed gave the team insight into the work required to design and analyze space environment protection for satellites.

### **6.1 Conclusions**

The Appleton CubeSat is designed to investigate the F layer of Earth's Ionosphere carrying the NASA designed Mini-INMS and GRIDS instruments. Appleton will be placed on a semi-Sun-synchronous elliptical orbit of Earth with a perigee of 180 km and an apogee of 600 km.

Performed thermal design and analysis to address Design Requirements 8.1 and 8.2. Evaluated the thermal loads onto Appleton from the Sun during a typical orbit using STK's Space Environment and Effects Tool (SEET). Used these thermal loads as inputs to COMSOL and performed thermal analysis on a de-featured CAD model of Appleton. In order to protect Appleton from the thermal environments of space, aluminized Mylar film was used to cover any openings in the aluminum frame. These sections of Mylar increased to high temperatures throughout the orbit of Appleton.

In addition, the internal thermal loads created by Appleton's components were evaluated using COMSOL. It was found that all components located inside of Appleton remained within the -20 – 50 °C thermal limit set in the design requirements of Appleton.

Results from the environmental analysis show that Appleton does not require additional radiation or particle shielding as the TID remains below the lower limit of component tolerances and the probability of damaging impacts is not significant over the mission duration. Appleton also has a minimal risk of damage due to spacecraft charging. The SPIS simulation using conditions present in the polar ionosphere resulted in the surface charging to a potential of between -1 to -2 Volts, increasing as more of the solar array is deployed. The COMSOL analysis suggests that the

design should include an external magnetometer to avoid internal interference from the magnetorquer when operating at its highest duty cycle.

## **6.2 Recommendations for Future Work**

After completing work designing protection for a CubeSat, the team has recommendations for future projects that attempt to complete similar tasks. Considering the mission constraints and requirements, the Appleton mission would require further simulation and testing before manufacture and launch planning.

## **6.3 Thermal Recommendations**

There are several methods to provide thermal protection to a satellite. Appleton uses passive thermal control methods in order to isolate its components from the ambient thermal environment by shielding its components. Passive thermal control methods were chosen in order to reduce complexity in the design and to reduce the complexity of the COMSOL model. Future MQPs should consider using an active thermal control method. An active control method will give the team more control over the internal environment of their spacecraft.

## **6.4 Space Environment Recommendations**

Future analysis should focus on the impact of auroral events on Appleton. These events are more difficult to predict and present abnormal concentrations of ionized particles and plasma, which may result in higher levels of spacecraft surface charging and an increased potential for damaging arcs. Additionally, a more detailed simulation of the spacecraft charging should be pursued as the simplified model does not account for the instrumentation on-board and how the environment would interact with these systems. Specifically, SPIS has the capacity to simulate particle measurement devices such as those in the payload and could be used to gauge the expected measurements from these devices such that they may be compared to those from an actual mission.

## 6.5 Social Impact – Space Debris

A growing concern in satellite design and one that was considered by this project is the effects of space debris. Space debris is the result of previous space missions that left objects in orbit (European Space Agency [ESA], 2020). Objects such as spent rocket stages and decommissioned satellites slowly accumulated in orbits around the Earth since the start of human involvement in space.

All of the objects in orbit around the Earth have the potential to collide with and damage operational satellites. Because of the threat that space debris causes, the United States Department of Defense’s global Space Surveillance Network (SSN) has tracked over 27,000 pieces of debris in near Earth orbit (Garcia, 2021). However, the objects that are of higher concern to NASA are the objects the SSN is unable to track due to their size. Small objects such as metal chips and paint flecks can cause damage due to their high orbital velocities, reaching over 25,000 kmh (Garcia, 2021). Figure 38 is a photo taken by astronaut Tim Peake of a crack in the Cupola window of the ISS. The crack was estimated to have been caused by a piece of space debris that was only a few thousandths of a millimeter in size (ESA, 2016).



Figure 38: Chip in International Space Station Cupola window (ESA, 2016).

In addition to small space debris objects, astronomers are also concerned about fragmentation events. A fragmentation event is when a man-made object in orbit breaks up in orbit, creating a large number of much smaller pieces of debris, that now all have their own orbital properties (ESA, 2020). A fragmentation event can occur in a variety of ways, from spacecraft colliding with each other, to explosions (intentional or unintentional), or even the conditions of space causing the object to break up (ESA, 2020). With a fragmentation event, there is the possibility to create thousands of new pieces of debris that may or may not be able to be tracked and increase the chances of an operational satellite to be impacted.

To prevent further build-up of space debris, satellites must be designed with end-of-life considerations. If satellites are launched without contingency plans for total mission loss (when communication and functionality of the satellite ceases due to environmental factors or design flaws) they will remain in an un-controlled orbit and contribute to an ever-growing number of man-made debris. To remain cognizant of the threat space debris poses on the future of Earth orbiting infrastructure, one of Appleton's primary requirements was to design a controlled de-orbit that would take the CubeSat into the atmosphere upon completion of the scientific mission. In doing so, Appleton will vaporize under the intense heat of re-entry thereby removing the possibility of Appleton contributing to orbital debris.

## 7. References

- Analytical Graphics, Inc. (AGI), "STK Space Environments Effects Tool (SEET)," 2020. [Online], Available: [https://help.agi.com/stk/11.0.1/stktraining/pdf/SEET\\_manual.pdf](https://help.agi.com/stk/11.0.1/stktraining/pdf/SEET_manual.pdf). [Accessed 22 February 2022].
- Anderson, C., Cuerdon, R., Kelsey, B., and Petilli, N., "Design and Analysis for a CubeSat Mission-III," Worcester Polytechnic Institute, Worcester, Massachusetts, 2020.
- Bograd, N., Jacobson, G., Kroyack, P., Lopez, C., and Peters, J., "Design and Analysis for CubeSat Missions," Worcester Polytechnic Institute, Worcester, 2018.
- Boushon, K. E., "Thermal analysis and control of small satellites in low Earth orbit," Missouri University of Science and Technology, Missouri, 2018.
- Brown, A., Cooley, W., Klenk, A., Messey, S., Meleti, J., Robatzek, A., St Jean, M., "Design of a NanoSat for an Ionospheric Mission," Worcester Polytechnic Institute, Worcester, Massachusetts, 2021.
- Community Coordinated Modeling Center (CCMC), Rastaetter, "International Reference Ionosphere - IRI (2016) with IGRF-13 coefficients". Retrieved February 14, 2022 from [https://ccmc.gsfc.nasa.gov/modelweb/models/iri2016\\_vitmo.php](https://ccmc.gsfc.nasa.gov/modelweb/models/iri2016_vitmo.php)
- Coker, R., "Thermal Modeling and Testing of the Edison Demonstration of Smallsat Networks Project," NASA, Huntsville, Alabama, 2014
- Dumbar, B., Hill, D., "About CubeSat Launch Initiative," NASA, 28 May 2020 [Online]. Available: <https://www.nasa.gov/content/about-cubesat-launch-initiative>. [Accessed 13 February 2022].
- Dumbar, B., Loff, S., "CubeSats Overview," NASA, 14 February 2018 [Online]. Available: [https://www.nasa.gov/mission\\_pages/cubesats/overview](https://www.nasa.gov/mission_pages/cubesats/overview). [Accessed 13 February 2022].
- Durgin, P., Karshina, V., Waring, S., "Design and Analysis for a CubeSat Mission," Worcester Polytechnic Institute, Worcester, Massachusetts, 2022
- European Space Agency, "Impact Chip," European Space Agency, 2016. [Online], Available: [https://www.esa.int/ESA\\_Multimedia/Images/2016/05/Impact\\_chip](https://www.esa.int/ESA_Multimedia/Images/2016/05/Impact_chip). [Accessed 28 February 2022].
- European Space Agency, "The current state of space debris," European Space Agency, 2020. [Online], Available: [https://www.esa.int/Safety\\_Security/Space\\_Debris/The\\_current\\_state\\_of\\_space\\_debris](https://www.esa.int/Safety_Security/Space_Debris/The_current_state_of_space_debris). [Accessed 28 February 2022].
- Gagnon, J., Tierney, D., Ritter, C., "Appleton Nanosat Critical Design Review," Worcester Polytechnic Institute, Worcester, Massachusetts, 2022.
- Garcia, M., "Space debris and Human spacecraft," NASA, 2021. [Online], Available: [https://www.nasa.gov/mission\\_pages/station/news/orbital\\_debris.html](https://www.nasa.gov/mission_pages/station/news/orbital_debris.html). [Accessed 28 February 2022].
- Garrett, H. B., Whittlesey, A. C., "Guide to Mitigating Spacecraft Charging Effects", John Wiley & Sons, Inc., Hoboken, New Jersey, 2012

Hatfield, M., "Dellinger: The Little CubeSat That Could," NASA, 23 October 2018. [Online]. Available: <https://www.nasa.gov/feature/goddard/2018/dellinger-the-little-cubesat-thatcould>. [Accessed 15 October 2021].

Hyun Ko, D., Laudage, Murphy, M., Pelgrift, D., and Young, S., "Design and Analysis of the Sphinx-NG CubeSat," Worcester Polytechnic Institute, Worcester, 2017.

"Ionosphere", Space Weather Prediction Center. (n.d.). [Online], Available: <https://www.swpc.noaa.gov/phenomena/ionosphere>. [Accessed: October 15, 2021]

Keesey, L., " NASA Team Pursues Blobs and Bubbles with New PetitSat Mission" NASA, 09 May 2017. [Online]. Available: <https://www.nasa.gov/feature/goddard/2017/nasa-team-pursues-blobs-and-bubbles-with-new-petitsat-mission> [Accessed 15 October 2021].

Klenzing, J., Davidson, R. L., Earle, G. D., Halford, A. J., Jones, S. L., Martinis, C. R., Paschalidis, N., Pfaff, R. F., Smith J. M., and Zawdie, K. A., "petitSat -A 6U CubeSat to examine the link between MSTIDS and ionospheric plasma density enhancements," in AGU 100 Advanced Earth and Space Science Fall Meeting, San Francisco, California, 2019.

Koontz S., "Spacecraft Charging: Hazard Causes, Hazard Effects, Hazard Controls", Video Seminar, (2018). Retrieved October 15, 2021, from <https://www.youtube.com/watch?v=N2ovNzg0zUI>

Missouri Institute of Science and Technology, Rolla, 2018.

"MODELS FOR GALACTIC COSMIC RAY AND SOLAR ENERGETIC PARTICLES AND THEIR APPLICATION TO SPACECRAFT DESIGN", James W. Adams, Jr, NASA Marshall Space Flight Center, Huntsville, AL, 2008

NASA CubeSat Launch Initiative, "CubeSat 101 Basic Concepts and Processes for First-Time CubeSat Developers", NASA, 2017.

NASA Earth Observatory, "Measuring Earth's Albedo," NASA Earth Observatory, [Online], Available: <https://earthobservatory.nasa.gov/images/84499/measuring-earths-albedo>. [Accessed 13 February 2022].

O'Bryan M., "Single Event Effects", November 5, 2015. Retrieved October 15, 2021, from <https://radhome.gsfc.nasa.gov/radhome/see.htm>

O'Bryan M., "Space Radiation Environment", December 1, 1998. Retrieved October 15, 2021, from <https://radhome.gsfc.nasa.gov/radhome/environ.htm>

O'Bryan M., "Total Ionizing Dose (TID) Effects", March 11, 2021. Retrieved October 15, 2021, from <https://radhome.gsfc.nasa.gov/radhome/tid.htm>

R. L. Davidson, B. Oborn, E. F. Robertson, S. Noel, G. D. Earle, J. Green, and J. Kramer, "The gridded retarding ion drift sensor for the petitSat CubeSat mission". Rev. Sci. Instrum. 91, 064502 (2020); <https://doi.org/10.1063/1.5140470> Submitted: 27 November 2019. Accepted: 20 May 2020. Published Online: 17 June 2020.

Rodriguez, M., Paschalidis, N., Jones, S., Sittler, N., Uribe, P., Chornay, D., and Cameron, T., "Miniaturized Ion and Neutral Mass Spectrometer for CubeSat Atmospheric Measurements," NASA Goddard Space Flight Center , Greenbelt, Maryland, 2016.

SpaceWeatherLive, "Historical Solar Cycles", n.d. Retrieved November 29, 2021, from <https://www.spaceweatherlive.com/en/solar-activity/solar-cycle/historical-solar-cycles.html>

"The Ionosphere", UCAR Center for Science and Education. (n.d.). Retrieved October 15, 2021, from <https://scied.ucar.edu/learning-zone/atmosphere/ionosphere>

The Nobel Prize, "Edward V. Appleton Facts," The Nobel Prize, 2022 [Online]. Available: <https://www.nobelprize.org/prizes/physics/1947/appleton/facts/> [Accessed 4 March 2022].

## 8. Appendix A: STK to COMSOL MATLAB Code

The code below was developed in MATLAB by former graduate student Harrison Hertlein for the purpose of converting STK data into csv files for COMSOL to read.

```
%%Preprocessing
clc
clear
%%Load in the .csv's from STK

eLEO4UCubeSatSolarIntensity=csvread('eLEO6UCubeSatSolarIntensity.csv',2,1);
eLEO4UCubeSatSunVectorsFixed=csvread('eLEO6UCubeSatSunVectorsFixed.csv',2,1);

%%Processing Solar Intensity

%Name of SI table
Name_SI =eLEO4UCubeSatSolarIntensity/100;

SI=Name_SI;

%%Processing Sun Vectors

%Name of SV table
Name_SV=eLEO4UCubeSatSunVectorsFixed;

%Create unit vectors

magnitude=sqrt(Name_SV(:,1).^2+Name_SV(:,2).^2+Name_SV(:,3).^2);

Name_SVxkm=Name_SV(:,1)./magnitude;
Name_SVykm=Name_SV(:,2)./magnitude;
Name_SVzkm=Name_SV(:,3)./magnitude;

%Translate into Body-Fixed Axis in COMSOL Model

xu=Name_SVykm;
yu=-Name_SVxkm;
zu=Name_SVzkm;

%Labeled as
VarNames= {'TimeEpSec', 'posx', 'negx', 'posy', 'negy', 'posz', 'negz'};
Suv=[xu yu zu];
Fn_u=[1 0 0; -1 0 0; 0 1 0; 0 -1 0; 0 0 1; 0 0 -1];
num=length(Suv);
cos_theta= zeros(1,6);
cos_theta_all=zeros(num,6);
for k=1:num
    for face=1:6
        cos_theta(k, face)= dot(Fn_u(face,:),Suv(k,:));
        if cos_theta(k, face)>0
            cos_theta(k, face)=cos_theta(k, face);
        else
            cos_theta(k, face)=0;
        end
    end
end
end

%Table Variables and Table
TimeEpSec=Name_SV(:,1);
posx=cos_theta(:,1);
negx=cos_theta(:,2);
posy=cos_theta(:,3);
negy=cos_theta(:,4);
posz=cos_theta(:,5);
negz=cos_theta(:,6);

cos_theta_xyz=table(TimeEpSec, posx,negx,posy,negy,posz,negz);
%%Save tables as a csv file

SI2=table(eLEO4UCubeSatSolarIntensity(:,1),SI);
writetable(SI2,'SI.csv')
writetable(cos_theta_xyz, 'cos_theta_xyz.csv')
```

## 9. Appendix B: Helmholtz Cage Instruction Manual

# Helmholtz Cage Instruction Manual

Recommended 2-3 people for assembly  
Assembly: Outside-In Method

### **Frame Pairs:**

NO and JOE = Inner vertical frame (X axis)

FRED and TED = Outside vertical frame (Y axis)

SMOL and PAUL = inner horizontal frame (Z axis)

*NOTE: Make sure to orient the coils so the plugs are closest to the power supply.*

*NOTE: For each pair make sure the arrows on the coil frame go the same direction.*

*NOTE: Each mounting bracket has two different sides, one with holes 5/8" from the edge of the bracket, and one with holes 3/8" from the edge of the bracket. Make sure to mount using correct side of the brackets so the holes align correctly.*

### **Frame Assembly:**

1. Attach brackets facing inwards on FRED and TED with pins.
2. Attach brackets facing inward on NO and JOE with pins, make sure to use the holes furthest from the corners.



Figure 39: NO and JOE

3. Stand NO and JOE up with the brackets on the two vertical sides.
4. Slot in either PAUL or SMOL between the bottom brackets of NO and JOE, secure with pins. Note: One bracket connection for SMOL has an ‘S’ on it and matches a customized bracket also labeled with an ‘S’.

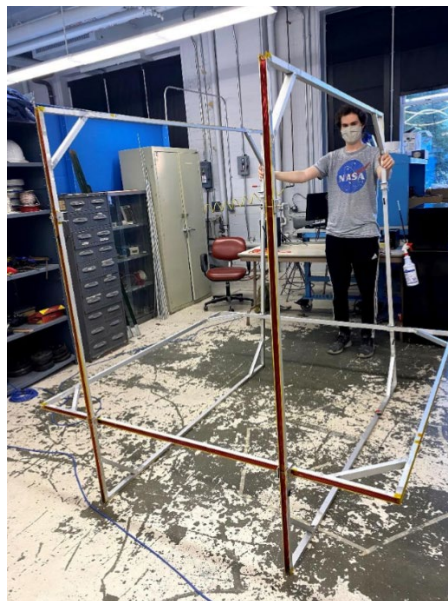


Figure 40: PAUL or SMOL connected to NO and JOE

5. Slot in either PAUL or SMOL (whichever is left) between the top brackets of NO and JOE, secure with pins.

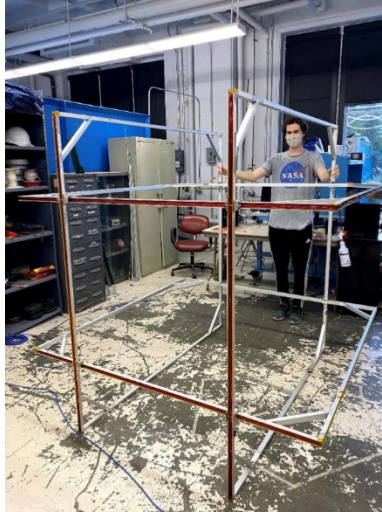


Figure 41: SMOL and PAUL connected to NO and JOE

6. Stand FRED or TED up with the brackets on the top and bottom.
7. Slightly lift the already connected frame and slide FRED or TED onto NO and JOE, secure with pins.

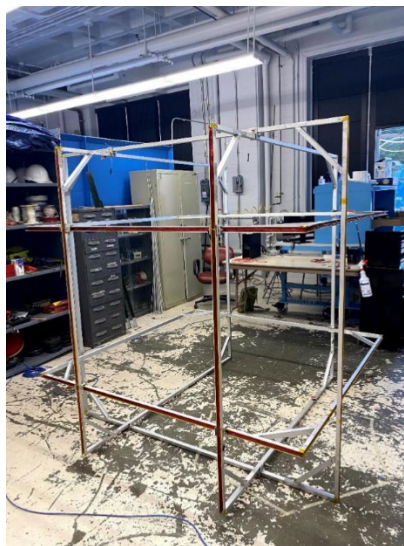


Figure 42: FRED or TED added to frame

8. Repeat steps 6 and 7 for the remaining coil of the pair FRED and TED.

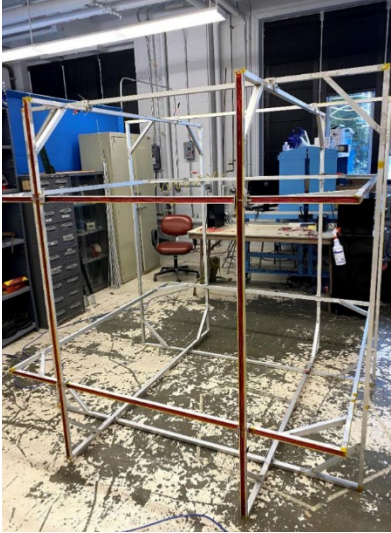


Figure 43: Full frame assembly

9. Slot the loose rubber pieces into the spaces of the brackets between the coils.



Figure 44: Bracket and rubber pieces

**Connection Set-Up:**

1. Connect labeled banana plug cables to corresponding coil plugs.

2. Connect the other ends of the cables for each coil pair to their corresponding splitter, based on the previously stated criteria.

NOTE: If coil arrow directions are opposite when assembled, attach one side as red-red and black-black and the other side as red-black and black-red.

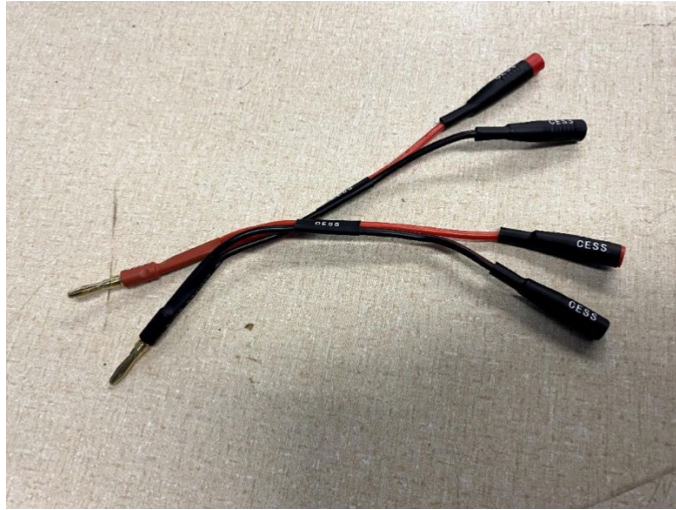


Figure 45: Splitter

### **LabJack/LabView integration:**

To be able to interact with LabJack with or without the use of LabView several steps need to be taken. To control LabJack directly from the computer:

1. An appropriate driver needs to be installed. This driver can be found by searching “U3 Quickstart for Windows Overview”.
2. Once the software package is installed the user will gain access to the LabJack control panel. LabJack Control Panel can communicate with LabJack connected via a USB, it allows to set inputs and outputs to analog and digital on different pins and control the voltage.

To integrate LabJack into LabView:

1. LabView needs to be installed, it can be downloaded through WPI Hub.

- LabJack uses a different driver than the one provided by National instruments, so before integrating LabJack with LabView the LabJackUD driver archive needs to be installed. This archive can be found by searching LABVIEW for UD on the LabJack website.
- The driver comes with example scripts, which can be used to test the LabJack connection (for example, U3 Read Serial Number is a good option, since the user will be able to tell if it works properly).
- To get a control panel of LabJack into LabView, install LabJack Utilities from Interface Innovations. This is a toolkit that allows you to set input/output types, record data and overall communicate with LabJack directly in LabView.
- This toolkit also comes with example code. Locate the National Instruments folder in Program Files (x86), then open LABVIEW 2021 folder > examples > Interface Innovations > LabJack Utilities > Basic Periodic Data Reader.
- A front Panel window will open (Figure 46). Below is a screenshot of the panel, change the circled values. In the example below a magnetometer was connected to pins FIO6 and FIO7, so they were switched to Analog Inputs, a different hardware set up will require a different software set up.

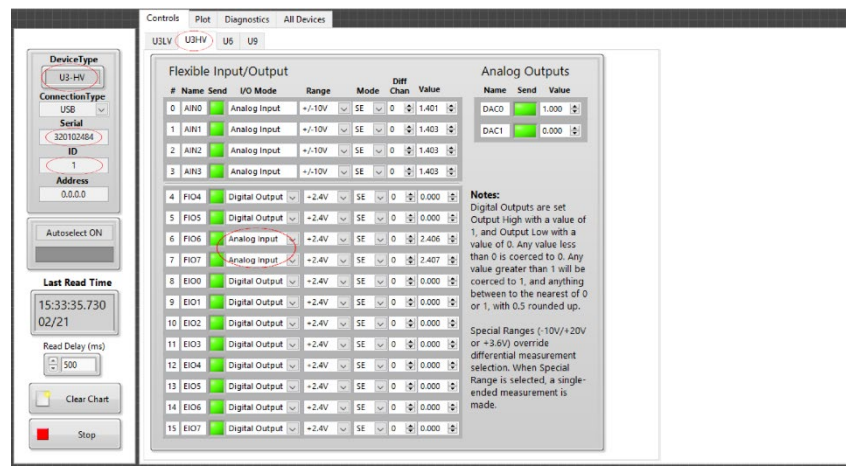


Figure 46: LabView – LabJack panel window

7. Once the setup is complete Run the code and click the Plot tab to see data being logged
8. To modify this code open Window > Show Block Diagram, which will open the visual representation of the code behind the front panel.